SURFACE FLUX FORMULATIONS IN THE COASTAL ZONE

Final report

Grant No. N00014-0-98-1-0282

Larry Mahrt
College of Oceanic and Atmospheric Sciences
Oregon State University
Corvallis, Oregon 97331

Prepared for:

REPORT DOCUMENTATION PAGE

1. AGENCY USE ONLY *(Leave Blank)*	2. REPORT DATE 14 Feb. 2000	3. REPORT TYPE AND DATES COVERED final

4. TITLE AND SUBTITLE
Surface Flux Formulations in the Coastal Zone

5. FUNDING NUMBERS
N00014-0-98-1-0282

6. AUTHORS
Larry Mahrt

7. PERFORMING ORGANIZATION NAME(S) AND ADDRESS(ES)
College of Oceanic and Atmospheric Sciences, Oregon State University, Corvallis, Oregon 97331

8. PERFORMING ORGANIZATION REPORT NUMBER

9. SPONSORING / MONITORING AGENCY NAME(S) AND ADDRESS(ES)
Atmospheric Modeling and Prediction, Office of Naval Research, Ballson Centre Tower One, 800 N. Quincy St., Arlington, VA 22217-5660

10. SPONSORING / MONITORING AGENCY REPORT NUMBER

11. SUPPLEMENTARY NOTES

12a. DISTRIBUTION / AVAILABILITY STATEMENT
Approved for public release

12b. DISTRIBUTION CODE

13. ABSTRACT *(Maximum 200 words)*

Surface Flux Formulations in the Coastal Zone

Eddy correlation and wave data from an offshore tower is analyzed. The data was collected during the Risoe Air Sea Experiment (RASEX). Interpretation of data analysis is made difficult by the fact that different influences are interrelated so that one can find significant, misleading, correlation through indirect relationships. The results do unambiguously indicate that shallow convective internal boundary layers in offshore flow suppress well developed convective eddies so that the heat flux is less than predicted by existing formulations; that is, the thin boundary-layer depth influences the flux-gradient relationship at the surface, requiring generalization of Monin-Obukhov similarity theory. The nature of the turbulence over land exerts a strong influence on both the boundary layer structure over the sea and the surface stress and fluxes through advection of turbulence energy. These effects are significant in the near coastal zone, typically the first 5 or 10 km offshore. Confused multimodel seas without a dominate spectral peak is a better indicator of large stress (large roughness length and large Charnock coefficient) than wave age. On the other hand, Monin-Obukhov similarity theory was a good approximation for the flux-gradient relationship for onshore flow. In general, there is no fundamental difficulty with Monin-Obukhov similarity.

14. SUBJECT TERMS
coastal zone, offshore flow, turbulent transport, air-sea interaction, surface sea stress, internal boundary layer

15. NUMBER OF PAGES
81

16. PRICE CODE

17. SECURITY CLASSIFICATION OF REPORT Unclassified	18. SECURITY CLASSIFICATION OF THIS PAGE Unclassified	19. SECURITY CLASSIFICATION OF ABSTRACT Unclassified	20. LIMITATION OF ABSTRACT

Surface Flux Formulations in the Coastal Zone

i

Introduction

The coastal zone is complicated by internal boundary layers and growing waves in offshore flow, incoming swell and shoaling, and diurnally varying wind fields. The case of offshore flow of warm air over cooler water (typically occurring in the afternoon) has alluded modeling efforts to date. Interpretation of data analysis is made difficult by the fact that different influences are interrelated so that one can find significant, misleading, correlation through indirect relationships. For example, the roughness length appears to be a strong function of wave age in offshore flow. However, wave age is strongly correlated with fetch, as is the strong turbulence advected from land, which decays in the downstream direction. Based on statistical analyses, one could highlight wave state as the dominate influence even though its effect is secondary and happens to correlate with the more direct influence of advection of turbulence on the surface stress.

With this warning, the present research has identified a number of solid influences. Shallow convective internal boundary layers in offshore flow suppress well developed convective eddies so that the heat flux is less than predicted by existing formulations; that is, the thin boundary-layer depth influences the flux-gradient relationship at the surface, requiring generalization of Monin-Obukhov similarity theory. The nature of the turbulence over land exerts a strong influence on both the boundary layer structure over the sea and the surface stress and fluxes through advection of turbulence energy. These effects are significant in the near coastal zone, typically the first 5 or 10 km offshore. Thirdly, confused multimodel seas without a dominate spectral peak is a better indicator of large stress (large roughness length and large Charnock coefficient) than wave age.

On the other hand, Monin-Obukhov similarity theory was a good approximation for the flux-gradient relationship for onshore flow. In general, there is no fundamental difficulty with Monin-Obukhov similarity for stationary homogeneous flow over the sea, in contrast to some earlier suspicions.

The following report consists of three papers from 1999, all based on data from the Risoe Air Sea Experiment (RASEX). "Observations of non-dimensional wind shear in the coastal zone" appeared in the *Quarterly Journal of Royal Meteorological Society* (vol. 128, pp 2685-2702). "Boundary-layer transitions in offshore flow has been recently submitted to *Boundary-Layer Meteorology*. "The coastal zone" recently appeared as a chapter in the book, *Air-Sea Exchange: Physics, Chemistry and Dynamics*, Kluwer Academic Publishers, 1999.

Boundary-layer transitions in offshore flow

L. Mahrt and Dean Vickers

College of Oceanic and Atmospheric Sciences
Oregon State University
Corvallis, OR 97331 USA
mahrt@oce.orst.edu

Jim Edson
Woods Hole Oceanographic Institute
Woods Hole, MA 02543, USA

James M. Wilczak
Environmental Technology Lab., ERL/NOAA
Boulder, CO 80303 USA

Jeff Hare
Cooperative Institute for Research in Environmental Sciences (CIRES)
University of Colorado
and Environmental Technology Lab., ERL/NOAA
Boulder, CO 80303 USA

Jørgen Høstrup
Risø National Laboratory
4000 Roskilde, Denmark

1

19 Sept 1999

Abstract

The adjustment of the boundary layer immediately downstream from a coastline is examined in terms of 2 levels of eddy correlation data collected on a mast at the shore and 6 levels of eddy correlation data collected from a mast 2 km offshore during RASEX. The characteristics of offshore flow are studied in terms of case studies and inter-variable relationships for the entire one month data set. A turbulent kinetic energy budget is constructed for each case study.

Although the buoyancy-generation of turbulence is generally small compared to shear-generation, the weakly stable and weakly unstable cases exhibit completely different vertical structure. With flow of warm air from land over cooler water, modest buoyancy destruction of turbulence and reduced shear-generation of turbulence over the less-rough sea surface cause the turbulence to weaken downstream from the coast. Shear-generation at higher levels and advection of stronger turbulence from land lead to a maximum of stress and turbulence energy above the surface, in contrast to conventional boundary layers where the stress is a maximum at the surface and decreases with height.

With flow of cool air over a warmer sea surface, a convective internal boundary layer develops downstream from the coast. However, an overlying thick layer of downward buoyancy flux (virtual temperature flux) is maintained by shear-generation in the accelerating offshore flow.

2

1. Introduction

The response of the atmosphere to surface discontinuities is often posed in terms of internal boundary layers (Garratt, 1990). In flow of warm air from a rough land surface over a cooler sea surface, the flow near the surface may not adjust to the new surface in the usual sense. The flow above the thin stable surface layer (Figure 1a), which was part of the boundary layer over land, may become partially decoupled from the surface, accelerate and form a low level jet (Smedman et al., 1995; Tjernström and Smedman, 1993). The shear on the underside of the jet may eventually generate turbulence and reestablish a surface-based boundary layer. In this case, the main source of turbulence is elevated and not at the surface and Monin-Obukhov scaling is invalid (Smedman et al., 1995). Further downstream, the flow can become near neutral as the air cools and substantially reduces the air-sea temperature difference (Smedman et al., 1997).

In some cases of flow of warm air over a cooler surface, a well-defined stable internal boundary layer develops (Garratt and Ryan, 1989). In a numerical study of the influence of the continental diurnal variation on offshore flow, Garratt (1987) found that the onset of daytime convective turbulence was advected offshore as a jump that could be traced for hundreds of kilometers offshore, well beyond the fetch in the present data. The numerical simulations of Mengelkamp (1991) indicate that the top of the stable internal boundary layer can be defined in terms of a minimum in the vertical profile of turbulence kinetic energy while numerical simulations of Garratt (1987) indicate a minimum of eddy diffusivity at the top of the stable internal boundary layer. The level of minimum turbulence separates the underlying internal boundary layer from overlying decaying turbulence. In Mengelkamp (1991),

3

this overlying decaying turbulence still exhibits some upward buoyancy flux offshore, characteristic of the upstream convective boundary layer.

A number of studies document development of well-defined convective internal boundary layers in flow of cool air over a warm surface (see review in Garratt, 1990). The growing convective internal boundary layer is usually capped by a thin entrainment zone of downward buoyancy flux. In contrast, Sun et al. (1998) study a convective internal boundary layer which is capped by a relatively thick layer of downward buoyancy flux, maintained by elevated shear-generation.

The above studies suggest complex and more varied vertical structure of the convective internal boundary layer in offshore flow. Sun et al. (2000) show that close to the coast, advection from land dominates the near-surface stress. We will refer to this region as the "near-coastal" zone (Figure 1). In offshore flow over the near-coastal zone, existing similarity theory may be invalid (Vickers and Mahrt, 1999). In contrast, Monin-Obukhov scaling successfully describes the turbulence energy budget (Edson and Fairall., 1998; Wilczak et al, 1999) and the flux-gradient relationship (Vickers and Mahrt, 1999) above the wave boundary layer for stationary onshore flow.

Downstream from the near-coastal zone, the stress is dominated by wave growth and advection of turbulence is no longer important. However, the atmospheric boundary-layer depth and vertical structure may still be adjusting. We refer to this region as the "outer coastal zone". This partitioning into two zones is somewhat arbitrary and over-simplified, and the various adjustments are gradual without a sharp transition in the downstream direction. In fact, definition of an internal boundary layer will not be obvious from the observations of stable offshore flows. However, this partitioning will help organize our initial investigations and provide some link to historical

thinking.

This study emphasizes the near-coastal zone and examines the vertical structure of both stable and unstable offshore flow with a heavily instrumented offshore tower, described in the next section.

2. Data

We analyze offshore tower data collected during the Risø Air Sea Experiment (RASEX). The full RASEX experiment instrumentation is described in Barthelmie et al. (1994) and Højstrup et al. (1997). In this study, we analyze observations taken at the sea mast west tower, located 2 km off the northwestern coast of the island of Lolland, Denmark, in 4 m of water, for the intensive observing period 3 October through 8 November 1994. The variation in mean water depth due to tides is only about 0.3 m. Local offshore (southerly) flow is characterized by a sea fetch ranging between 2 km and 5 km. On-shore flow has a fetch between 15 km and 25 km as it travels across an inland sea, and is still potentially fetch-limited. Fetch is the distance along the flow from the coast to the sea mast. Water depths for the longer fetches range from 4 m to 20 m. The nearby land surface is relatively flat.

Various corrections to the data are recorded in Mahrt et al. (1996). Averaged vertical profiles of the buoyancy flux and friction velocity are computed from the 6 levels of sonic anemometers. In offshore flow, the vertical variation of the flux is much larger than differences between individual sonic anemometers. For some analyses, the fluxes for the three lowest levels will be averaged since the effect of instrumental differences may be larger than the actual vertical variation over such short vertical distances.

5

2.1 Turbulence energy budget

Insight into the vertical structure of the offshore flow can be gained by evaluating the turbulence kinetic energy budget using the stress and virtual temperature flux computed from sonic anemometers located at 3, 6, 10, 18, 32 and 45 m on the offshore tower.

For shear-generation of turbulence kinetic energy, the mean wind shear is computed from seven cup anemometers (P224b sensor) located at 7, 15, 20, 29, 38, 43 and 48 m. Corrections to the cup anemometers were made by compositing the wind speed profile based on all of the records with fetch greater than 10 km and near-neutral conditions (abs.(z/L) < 0.1). This averaged profile is fit to a log-linear height-dependence and percentage corrections for each level are constructed from the deviation of the averaged profile from the log-linear fit. These corrections partially remove small systematic irregularities in the profile. Percentage corrections to the wind speed are always less than 2% but exert a greater influence on the shear. The computation of the shear-generation term neglects directional shear, which could not be adequately estimated from the sonic anemometer data due to small uncertainties in orientation.

For offshore cases (fetch < $5km$), advection of turbulence kinetic energy is estimated as

$$V[\frac{TKE_{SM} - TKE_{LM}}{fetch}] \tag{1}$$

where V is the wind speed, SM refers to the offshore mast and LM refers to the land mast. This term can be estimated at the 6- and 18-m levels, corresponding to the common sonic anemometer levels at the landmast and seamast. Here, it is assumed that the turbulence kinetic energy, TKE, is spatially invariant along the coast for cases where the flow was not perpen-

dicular to the coast. Unfortunately, advection could not be estimated above 18 m. Dissipation is estimated following the spectral approach of Edson and Fairall (1998). The spectral slope was determined from a least squares fit over the frequency range thought to be in the inertial subrange. In some cases, the inertial subrange does not appear to be fully developed possibly due to nonequilibrium conditions in offshore flow and errors in the dissipation estimate may be significant. We expect the wave-induced pressure transport term to be small for this data even at the lowest (3 m) tower level (Hare et al., 1997). The wavelength and amplitude of the fetch-limited surface waves are generally small compared to open ocean values.

The residuals for the turbulence kinetic energy budget are expected to be large because the pressure transport term is neglected and the errors in the vertical flux divergence and horizontal advection of turbulence energy are expected to be significant. The vertical flux divergence term (triple correlation term) suffer larger random flux errors compared to covariances, and the flux divergence term is a small difference between vertical flux of turbulence energy at two levels. We have also neglected the Eulerian time-dependence term, the mean vertical advection of turbulence kinetic energy as well as horizontal flux divergence of turbulence energy equation. These terms appear to be small with relatively large errors. Considering the above difficulties, the residual term is relatively small for most of the case studies (see Figures 6 and 11 below).

2.2 Diagnostic quantities

To crudely quantify the unusual vertical structure of offshore flows, the stress ratio is computed as

7

$$stress\ ratio = \frac{stress_{upper}}{stress_{lower}} \tag{2}$$

where $stress_{upper}$ is the average of the stress magnitude at the two upper tower levels, 32 m and 45 m, and the $stress_{lower}$ is the average of the three lowest levels, 3 m, 6 m and 10 m.

We compute the buoyancy flux ratio as

$$buoyancy\ flux\ ratio = \frac{buoyancy flux_{upper}}{buoyancy flux_{lower}} \tag{3}$$

where the same levels are used as in Eq. 2. This relationship is applied only to data where the magnitude of the buoyancy flux for the lower layer exceeds $0.01\ °Cms^{-1}$.

2.3 External variables

We now define two variables which are external to the vertical structure of the flow at the sea mast. With the exception of flow of cold air over warmer water, the turbulence will decay to some smaller value downstream from the coast. The *travel time* of the flow (fetch/wind speed) from the coast describes the period during which the decay takes place.

As a second external variable, we define an "external Richardson number"

$$R_{ext} \equiv \frac{hg\Delta\theta/\Theta_o}{\alpha\sigma_w^2} \tag{4}$$

where h is the boundary-layer depth, σ_w is the standard deviation of the upstream vertical velocity, $\Delta\theta$ is the difference between the upstream air temperature and the downstream sea surface temperature, Θ_o is the averaged potential temperature, g is the acceleration of gravity and α is a nondimen-

8

sional coefficient, arbitrarily chosen as 10^3 in order to make R_{ext} of order one.

With small values of R_{ext}, the strength of the potential air-surface temperature difference is not sufficient to induce a well-defined internal boundary layer in the face of vigorous mixing (large σ_w) due to the advected turbulence. In this case, the boundary layer advected from land is predicted to adjust to the new surface conditions through continuous decrease of turbulence and boundary-layer depth in the downstream direction, without formation of a new internal boundary layer (Figure 1c). We refer to this case as the adjusting boundary layer. While windy cases of small air-sea temperature difference appear to fit this category, the RASEX does not allow examination of the spatial variation of the boundary layer depth. R_{ext} is an external forcing parameter representing the influence of the upstream flow and sea surface temperature, as opposed to the Richardson number and z/L over the sea which are functions of the flow itself at the seamast.

This external Richardson number can be evaluated only for offshore flow (fetch = 2-5 km) where the landmast can be used as upstream information. The boundary-layer depth was available from a tethered balloon only for a subset of days. We assign the boundary-layer depth a constant value of 500 m, in which case R_{ext} depends only on the temperature difference and upstream σ_w. The latter was estimated as the average from the 6- and 18-m levels at the landmast. The usual stability parameter z/L is highly correlated with R_{ext} (Figure 2) for stable, near neutral and weakly unstable conditions, perhaps reflecting the fact that the local stability is determined by advection from the upstream land surface. Once R_{ext} becomes more negative than -1, z/L appears to be independent of R_{ext}, although there were no offshore cases with large instability.

9

3. Land-sea contrast

Even though the observations are collected in October at 54 N latitude, some diurnal signature can be seen on many of the days with offshore flow. The maximum upward buoyancy flux at the sea surface most often occurs in the morning when the air advected from the land is coolest. The maximum downward buoyancy flux at the sea surface tends to occur in the late afternoon when the air over land is warmest. On average, the diurnal amplitude of the buoyancy flux is 0.02 $°Cms^{-1}$. This averaged diurnal amplitude is reduced by the low sun angle and numerous cloudy days included in the average. Using temperature at two levels for summer for the same land and sea masts, Barthelmie et al. (1996) found, on average, stable conditions over the water during the day and unstable conditions at night.

For offshore flow for both stable ($R_{ext} > 0$) and unstable conditions ($R_{ext} < 0$), the surface stress at the sea mast has typically decreased by a factor of two compared to the land surface stress (30% decrease of friction velocity, Figure 3a,b), and the offshore flow typically accelerates 1-2 ms^{-1} over the fetch of a few kilometers. The exception is for small stress over land and instability over the sea (Figure 3b), when the stress is sometimes greater over the sea than over the land. Excluding these cases, the stress over the sea is highly correlated with the stress at the landmast, in spite of some variation of fetch and upstream land conditions. However, much of this correlation is through the dependence of the stress on wind speed.

The characteristics of the offshore flow are more systematically related to travel time than fetch in terms of the scatter in Figures 7, 8, 12 and 13 in the following sections, suggesting that the flow is influenced by an internal decay time scale. The turbulence may decay more near the surface where the travel

10

time to the tower is longer (weaker wind near the surface) and the dissipation time scale is shorter (smaller turbulent length scale near the surface). For offshore flow, the travel times at the offshore mast generally range between a few hundred seconds and about 600 seconds. The decay time of convective turbulence can be estimated in terms of the ratio of the vertical length scale of the turbulence divided by the velocity scale of the turbulence. Nieuwstadt and Brost (1986) and Sorbjan (1997) provide specific formulations for the case where the velocity scale is the free convection velocity and the length scale is the depth of the convective mixed layer. Applying such a relationship to the few RASEX cases with convective conditions over land predicts a decay time scale on the "order" of ten minutes, which is consistent with the observed variation of turbulence quantities with travel time in Sections 4 and 5. In contrast, existing formulations of the surface stress in offshore flow are formulated in terms of a nondimensional fetch (Perrie and Toulany, 1990; Vickers and Mahrt, 1997). More data is required before a new formulation can be constructed in terms of travel time.

4. Upward buoyancy flux from the sea surface

We now analyze the flow of cool air over a warmer surface in terms of three periods when the buoyancy flux at the surface exceeds 0.01 $°Cms^{-1}$ for more than a half day (Table 1). All three cases are characterized by very weak instability. The time-height cross-section (Figure 4) shows diurnal variation with maximum upward buoyancy flux in the morning due to advection of cool air from land. The vertical profiles are averaged over all of the one-hour records for each of the three cases (Figure 5). The turbulence energy budget is averaged over the same data. The residuals of the turbulence energy budgets

11

(Figure 6) are reasonably small considering the possible substantial errors in certain terms of the budget and omission of the pressure transport term (Section 2.1). Error bars for the averaged profiles are not shown because much of the variation within the averaging period is due to either diurnal trend or other nonstationarity, rather than random variations. The analysis in this section also considers statistics based on all of the individual one-hour records within the entire field program when $z/L < -0.1$.

Table 1. CASE STUDIES. B.F. is the surface buoyancy flux ($°Cms^{-1}$), "travel" refers to the travel time in minutes and fetch is in kilometers. Case I for the stable and unstable flows include time-height cross-sections of the buoyancy flux (Figures 4 and 9).

case study	Time (DOY)	travel	fetch	B.F.	wind ms^{-1}	z/L
unstable-UI	291.9 - 293.0	5	3	0.02	10	-0.10
unstable-UII	289.25 - 290	35	18	0.03	9	-0.11
unstable-UIII	307.7 - 308.35	4.5	2.8	0.01	10	-0.02
stable-SI	297.0 - 297.7	5	2	-0.02	7	0.44
stable-SII	299.0 - 301.0	6	2.8	-0.01	8	0.06
stable-SIII	303.15 - 303.25	5	2	-0.01	6.5	0.11

4.1 Thick capping layer of downward buoyancy flux

In RASEX, offshore flow of cool air over warmer water for short travel times (near-coastal zone) is generally characterized by a layer of upward buoyancy flux capped by a relatively thick layer of downward buoyancy flux (Case UI, Figure 5a and Case UIII, Figure 5c), as also observed in Sun et al., (1998) in flow of cool air over a warmer lake. The momentum flux in

12

the overlying layer of downward buoyancy flux is comparable to that near the surface. These characteristics contrast with the textbook picture of a convective internal boundary layer where the layer of upward buoyancy flux is capped by a thin entrainment zone of downward buoyancy flux and the momentum flux decreases with height across the convective boundary layer.

The buoyancy-generation of turbulence energy is quite small compared to the shear-generation and dissipation (Figure 6). The horizontal advection of turbulence energy is also small in the turbulence energy budget, at least near the surface where it could be evaluated (Figure 6a, c). The horizontal advection term is a little larger for stable cases (Figure 11, Section 5). Horizontal advection presumably becomes increasingly important at higher levels and also shoreward of the seamast. The main effect of advection may be through advection of temperature and stress. The advected stress in turn enhances momentum transfer to the sea surface and subsequently enhances wave growth compared to what would occur without advection of stress. The importance of advection of stress is partly inferred from numerical studies, which will be reported in a future publication.

For the two short fetch cases (near-coastal zone flow), the turbulent transport term is positive near the surface (Figure 6), associated with convergence of downward flux of turbulence energy (not shown). For the long fetch case (outer coastal zone), the vertical flux term is negative near the surface corresponding to traditional export of turbulence energy upward out of the surface layer.

In contrast to the short fetch cases, the flow in Case UII reaches the tower after a relatively long fetch of 18 km and travel time of about 35 min. The offshore tower is now in the outer coastal zone with respect to the flow direction. The flow is unstable at all levels and the momentum

13

flux for Case UII (Figure 5b) is approximately constant with height, within the uncertainty due to differences between different sonic anemometers. The unstable internal boundary layer is deep compared to the tower layer because of the longer travel time over the water. The buoyancy flux is small and erratic for this case due to small air-sea temperature difference and the flux shows no obvious trend with height.

To further examine the bulk vertical structure, consider the ratio of the buoyancy flux in the upper part of the tower layer to that in the lower part of the tower layer (Eq. 3) for all of the records with upward surface buoyancy flux when $z/L < -0.1$. The buoyancy flux ratio (Figure 7) for short offshore travel times of less than ten minutes (near coastal zone) is generally less than one, indicating that the internal boundary layer is shallow and the buoyancy flux decreases significantly across the tower layer. In fact, the buoyancy flux ratio is negative for a subset of the short fetch cases, as occurred in two of the case studies. With negative values, the convective internal boundary layer is so thin that the upper part of the tower layer is characterized by downward buoyancy flux. The downward buoyancy flux occurs over a relatively thick layer, which probably extends above the tower layer.

For travel times longer than 10 minutes (outer coastal zone), the buoyancy ratio is always positive and is typically of order one with large scatter. That is, the buoyancy flux decreases only slowly with height implying that the internal boundary layer is deep compared to the tower layer.

The turbulent transport of turbulence energy (Figure 8) is often large upward for unstable cases with short travel time of less than 300s (near coastal zone) where advection from land is most important. For stable offshore flow, the pattern is quite different (next section).

14

5. Downward buoyancy flux

Flow of warm air over a cooler surface is now analyzed in terms of three case study periods where the magnitude of the downward buoyancy flux at the surface is greater than 0.01 $°Cms^{-1}$ for most of the episode. The time-height cross-section for the buoyancy flux is shown for the case with the largest sustained downward buoyancy flux (Figure 9), while the vertical structure is averaged for all of the one-hour records in each of the three cases (Figures 10a,b,d, 11 a-c). All three cases correspond to short fetch and short travel time (Table 1). We will also analyze statistics based on all of the individual one-hour records during the entire field program when $z/L > 0.1$.

For Case SI, the downward buoyancy flux at the sea surface is due to advection of warm air from the heated land surface over the cooler water and exhibits significant diurnal variation. In Cases SI and SII, the buoyancy flux is weak downward in the lowest 20-30 m and then becomes generally negligible at higher levels (Figures 9, 10a,d).

5.1 Elevated stress maximum

Above the thin surface layer of downward buoyancy flux, the stress and vertical velocity variance are 20-60% larger than near the surface, as can be determined from Figure 10 by squaring u_* and σ_w. The stress reaches a maximum in the upper part of the tower layer for Cases SI and SII (Figure 10a,c) while the stress and turbulence energy slowly increase with height throughout the tower layer for Case SIII, implying maximum values above the tower (Figure 10d). For shorter periods, the stress near the surface may nearly collapse, as occurred for the one-hour subperiod of Case SI (Figure 10b) where the

15

measured stress and downward heat flux are essentially zero within measurement error. The averaged vertical structure in Cases SI-SIII is quite different from that in traditional stable boundary layers where the stress, buoyancy flux and turbulence energy decrease monotonically with height (Caughey et al., 1979; Lenschow et al., 1987; Sorbjan, 1988). In the present observations of offshore flow, the elevated maxima of stress and turbulence energy are maintained by shear-generation and presumably augmented by advection of stronger turbulence from land (Section 5.2).

The stress convergence below the elevated stress maximum acts to accelerate the flow and may account for much of the observed flow acceleration downstream from the coast. The observed vertical convergence of stress at the sea mast, applied over the travel time from the coast, corresponds to an acceleration of 0.5-1.0 ms^{-1}. The observed acceleration ranged from 0.8 - 1.3 ms^{-1}. A rigorous assessment of the momentum budget is prevented by inadequate assessment of the local horizontal pressure gradient.

The observed increase of stress with height does not appear to be related to instrumentation differences. For long-fetch, near-neutral conditions, the observed stress is essentially constant with height across the tower layer (or decreases very slowly with height), as expected in non-advective traditional boundary layers where the boundary layer is much deeper than the tower layer.

An elevated stress maximum is also observed by Glendening (personal communication) in an LES model of flow from a rough surface to a smooth surface with zero buoyancy flux. He used this elevated stress maximum to define the top of the new internal boundary layer. The elevated maximum was maintained by horizontal advection. Definition of the top of the internal boundary layer in terms of a stress maximum contrasts sharply with defi-

16

nition of the top of the internal boundary layer in terms of a minimum of turbulence cited in the Introduction. The differences of the vertical structure may be due to different relative position downstream from the surface change. The present observations in offshore flow are short fetch (near-coastal zone) and Mengelkamp (1991) finds that the minimum develops after a certain distance offshore.

We now examine the ratio of stress in the upper part of the tower layer to that in the lower part of the tower layer (Eq. 2) for all of the one-hour records where $z/L > 0.1$. The momentum flux ratio is often large for small travel time, exceeding two in a significant fraction of the cases (Figure 12). These values correspond to a rapid increase of stress with height. The momentum flux ratio decreases rapidly with increasing travel time to values closer to unity for travel times of ten minutes and longer, although the scatter is large. For values near unity, the stress decreases slowly with height, implying that the internal boundary layer is deep compared to the tower layer.

5.2 Downward transport of turbulence; upside-down boundary layer

For Cases SI and SIII, the vertical turbulent transport of turbulence kinetic energy is significant downward (not shown), implying that the main source of turbulent kinetic energy is elevated. This downward transport of turbulence energy is consistent with the increase of turbulence and stress with height, in contrast to the usual boundary layer. The downward transport of turbulence kinetic energy leads to significant vertical flux convergence of turbulence energy at the lower levels (Figure 11). The turbulence near the surface is therefore partly maintained by downward transport of turbulence

17

energy. For Case SII, the height-dependence of the turbulent transport is irregular.

Cases of large elevated generation of turbulence and downward transport will be referred to as "upside-down" boundary layers in recognition of the top-down transport of turbulence energy. In contrast to the classification in Mahrt (1999), the upside-down boundary layer in the present offshore flow occurs with relatively weak stability and is apparently partly maintained by horizontal advection. The downward transport of turbulence toward the surface may be augmented by the pressure transport term in the turbulence kinetic energy equation (Smedman et al., 1995).

Considering all of the stable one-hour records, the vertical transport of turbulence energy for short travel times is often large positive (Figure 13), as also occurred in the unstable offshore flow cases. These larger values are apparently associated with advection from land. In contrast to unstable conditions, the vertical transport of turbulence energy is sometimes large downward for short travel times less than 300 s (Figure 13), again implying that the strongest generation of turbulence is elevated in some stable offshore flows in the near coastal zone. These cases of downward transport of turbulence energy normally correspond to an increase of stress with height (Figure 14, momentum flux ratio > 1).

What generates the upside-down structure? Firstly, the shear-generation term tends to increase with height (Figure 11) in contrast to the usual boundary layer where it decreases rapidly with height. Secondly, the turbulence advected horizontally from land in offshore flow is thought to decay more slowly at higher levels where the turbulence length scale is larger and travel time is shorter (stronger wind speed). The dissipation rate divided by the turbulence energy decreases with height for both stable and unstable cases.

Finally, the advection of stress is expected to increase with height. These expectations are based on numerical simulations, to be reported in a separate manuscript.

6. Conclusions

For the present data, weakly convective internal boundary layers in flow of cooler air over warmer water are generally capped by a thick layer of downward buoyancy flux in the near coastal zone. Here, the vertically integrated buoyancy flux is small or even negative and the vertically-integrated turbulence is driven by shear-generation.

With advection of warm air over cooler water in the near coastal zone, the vertical structure may be quite different than that expected from traditional conceptual models of the internal boundary layer, even though the flow is only modestly stable ($z/L < 0.5$). These cases most often occur in the afternoon with flow of warm air from the heated land surface. In some cases, the turbulence energy and stress increase with height, reaching an elevated maximum, and the transport of turbulence energy is downward toward the surface. We have referred to these cases as "upside-down boundary layers". The increase of stress with height appears to be maintained by horizontal advection from land and shear-generation associated with accelerating flow over the water. This upside-down structure was observed with travel times less than 10 minutes (fetches generally less than 5 km), here referred to as the near-coastal zone.

19

References

Barthelmie, R. J., Courtney, M. S., Højstrup, J., and Sanderhoff, P.: 1994, 'The Vindeby Project: A Description', Report R-741(EN), Risø National Laboratory, DK4000, Roskilde, Denmark.

Barthelmie, R. J., Grisogono, B., and Pryor, S. C.: 1996, 'Observations and Simulations of Diurnal Cycles of Near-Surface Wind Speeds over Land and Sea', *J. Geophys. Res.*, **101**, 21,327-21,337.

Caughey, S. J., Wyngaard, J. C., and Kaimal, J. C.: 1979, 'Turbulence in the Evolving Stable Boundary Layer', *J. Atmos. Sci.*, **36**, 1041-1052.

Edson, J. and Fairall, C. W.: 1998, 'Similarity Relationships in the Marine Atmospheric Surface Layer for Terms in the TKE and Scalar Variance Budgets', *J. Atmos. Sci.*, **55**, 2311-2328.

Garratt, J. R.: 1987, 'The Stably Stratified Internal Boundary Layer for Steady and Diurnally Varying Offshore Flow', *Boundary-Layer Meteorol.*, **38**, 369-394.

Garratt, J. R.: 1990, 'The Internal Boundary Layer - a Review', *Boundary-Layer Meteorol.*, **50**, 171-203.

Garratt, J. R. and Ryan, B. F.: 1989, 'The Structure of the Stably Stratified Internal Boundary Layer in Offshore Flow over the Sea', *Boundary-Layer Meteorol.*, **47**, 17 - 40.

Hare, J. E., Hara, T., Edson, J. B., and Wilczak, J. M.: 1997, 'A Similarity Analysis of the Structure of Airflow over Surface Waves', *J. Phy. Oc.*, **27**, 1018-1037.

Højstrup, J., Edson, J., Hare, J., Courtney, M. S., and Sanderhoff, P.: 1997, 'The RASEX 1994 Experiments', Risø -R-788, Risø National Laboratory, Roskilde, Denmark, (ISBN-87-550-2039-9), 24 pp.

Lenschow, D. H., Li, X. S., Zhu, C. J., and Stankov, B. B.: 1987, 'The Stably Stratified Boundary Layer over the Great Plains. I. Mean and Turbulence Structure', *Boundary-Layer Meteorol.*, **42**, 95-121.

Mahrt, L.: 1999, 'Stratified Atmospheric Boundary Layers', *Boundary-Layer Meteorol.*, **90**, 375-396.

Mahrt, L., Vickers, D., Howell, J., Højstrup, J., Wilczak, J. A., Edson, J., and Hare, J.: 1996, 'Sea Surface Drag Coefficients in RASEX', *J. Geophys. Res.*, **101**, 14327-14335.

Mengelkamp, H.-T.: 1991, 'Boundary Layer Structure over an Inhomogeneous Surface: Simulation with a Non-Hydrostatic Mesoscale Model', *Boundary-Layer Meteorol.*, **57**, 323-342.

Nieuwstadt, F. and Brost, R.: 1986, 'The Decay of Convective Turbulence', *J. Atmos. Sci.*, **43**,532-546.

Perrie, W. and Toulany, B.: 1990, 'Fetch Relations for Wind-Generated Waves as a Function of Wind-Stress Scaling', *J. Phy. Oc.*, **20**, 1666-1681.

Smedman, A.-S., Bergström, H., and Högström, U.: 1995, 'Spectra, Variances and Length Scales in a Marine Stable Boundary Layer Dominated by a Low Level Jet', *Boundary-Layer Meteorol.* **76**, 211-232.

Smedman, A.-S., Bergström, H., and Grisogano, B.: 1997, 'Evolution of Stable Internal Boundary Layers Over a Cold Sea', *J. Geophys. Res.* **102**, 1091-1099.

Sorbjan, Z.: 1988, 'Structure of the Stably-Stratified Boundary Layer During the SESAME-1979 Experiment', *Boundary-Layer Meteorol.* **44**, 255-266.

Sorbjan, Z.: 1997, 'Decay of Convective Turbulence Revisited', *Boundary-Layer Meteorol.*, **82**, 501-515.

Sun, J., Desjardins, R., Mahrt, L., and MacPherson, J. I.: 1998, 'Transport of Carbon Dioxide, Water Vapor and Ozone by Turbulence and Local Circulations', *J. Geophys. Res.*, **103**, 25,873-25,885.

Sun, J., Vandemark, D., Mahrt, L., Vickers, D., Crawford, T., Vogel, C., and Dumas, E.: 2000, 'Momentum Transfer over the Coastal Zone', Submitted to *J. Geophys. Res.*.

Tjernström, M. and Smedman, A.-S.: 1993, 'The Vertical Structure of the Coastal Marine Atmospheric Boundary Layer', *J. Geophys. Res.*, **98**, 4809-4826.

Vickers, D. and Mahrt, L.: 1997, 'Fetch Limited Drag Coefficients over Shallow Water', *Boundary-Layer Meteorol.*, **89**, 53-79.

Vickers, D. and Mahrt, L.: 1999, 'Observations of Nondimensional Shear in the Coastal Zone', To appear in *Quart. J. Roy. Met. Soc.*.

Wilczak, J., Edson, J., Jøstrup, J., and Hara, T.: 1999, 'The Budget of Turbulent Kinetic Energy in the Marine Atmospheric Surface Layer', *Air-Sea Exchange - Physics, Chemistry, Dynamics and Statistics*, Kluwer, Ed. G. Geernaert.

Figure legends

Figure 1. Hypothesized two-layer structure for offshore flow. a) Flow of warmer air over a cooler surface. The downward-pointing area indicates the possibility of downward transport of turbulence energy. b) Flow of cooler air over a warmer surface. c) Small air-sea temperature difference. The phase speed of the wind driven waves (C_p) increases in the offshore direction. The values of offshore travel time for partitioning the near-coastal zone, outer coastal zone and near-equililbrium region are based on analyses in Section 4-5. Transitions are gradual and travel time values probably vary dramatically between different situations.

Figure 2. Relationship of the stability z/L to the external Richardson number (Eq. 4) for all of the short fetch one-hour records.

Figure 3. Relationship of the offshore friction velocity (ms^{-1}) to the land-mast value for unstable (a) and stable (b) conditions.

Figure 4. Time-height cross-section for unstable case UI for the buoyancy flux ($°Cms^{-1}$) where darker areas correspond to upward buoyancy flux. Times are GMT which is one hour behind local solar time.

22

Figure 5a-c. Vertical profiles of the friction velocity (ms^{-1}), buoyancy flux ($^{\circ}Cms^{-1}$) and σ_w (m^2s^{-2}) for the three unstable cases.

Figure 6a-c. The turbulence energy budget (m^2s^{-3}) for the unstable cases. A is the advection term, ϵ the dissipation, S the shear-generation term, F the vertical divergence of the flux of the turbulence energy, B the buoyancy-generation term and R, the residual.

Figure 7. Buoyancy flux ratio (Eq. 3) as a function of travel time for all of the unstable records ($z/L < -0.1$) .

Figure 8. The dependence of the vertical flux of turbulence energy (m^3s^{-3}) at 18 m on travel time for all of the one-hour records with fetch values less than 5 km for unstable conditions ($z/L < -0.1$).

Figure 9. Time-height cross-section of the buoyancy flux ($^{\circ}Cms^{-1}$) for stable case SI where lighter areas correspond to stronger downward buoyancy flux. Times are GMT which is one hour behind local solar time.

Figure 10. Vertical profiles of the friction velocity (ms^{-1}), buoyancy flux ($^{\circ}Cms^{-1}$) and σ_w (ms^{-1}) for the three stable cases (a, c, d) and for a one-hour subperiod during case SI where fluxes are very weak (panel b).

Figure 11. The turbulence energy budget ($10^{-3}m^2s^{-3}$) for the three stable Cases (a-c). A is the advection term, ϵ the dissipation, S the shear- genera-tion term, F the vertical divergence of the flux of the turbulence energy, B the buoyancy-generation term and R, the residual.

Figure 12. The stress ratio (Eq. 2) as a function of travel time for all of the one-hour records with stable conditions ($z/L > 0.1$).

Figure 13. The dependence of the vertical flux of turbulence energy ($m^3 s^{-3}$) at 18 m on travel time for all of the one-hour records with stable conditions ($z/L > 0.1$).

Figure 14. The relationship between the turbulence energy flux ($m^3 s^{-3}$) at 18 m and the momentum flux ratio for stable conditions based on bin-averaged values computed from the one-hour records. Also shown are standard error bars.

Figure 1. Hypothesized two-layer structure for offshore flow. a) Flow of warmer air over a cooler surface. The downward-pointing arrow indicates the possibility of downward transport of turbulence energy. b) Flow of cooler air over a warmer surface. c) Small air-sea temperature difference. The phase speed of the wind-driven waves (C_p) increases in the offshore direction. The values of offshore travel time for partitioning the near-coastal zone, outer coastal zone and near-equilibrium region are based on analyses in Section 4-5. Transitions are gradual and travel time values probably vary dramatically between different situations.
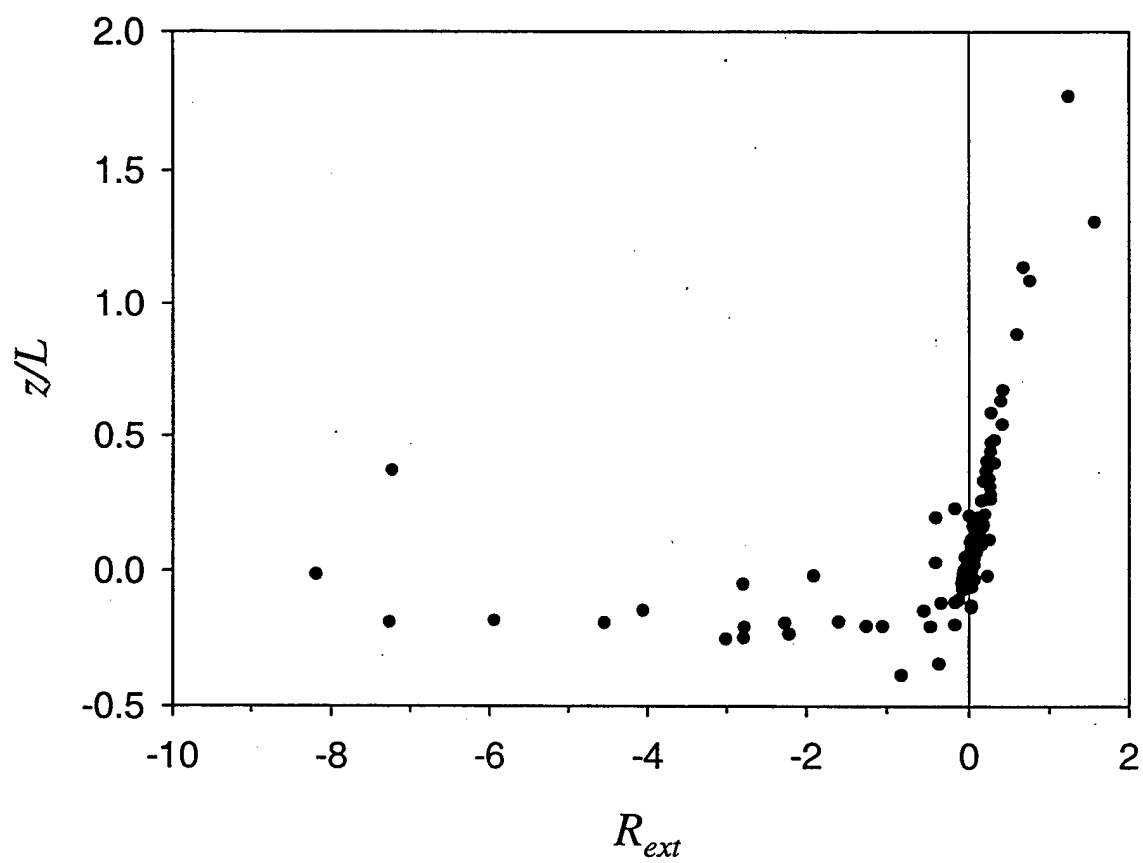
Figure 2. Relationship of the stability z/L to the external Richardson number (Eq. 4) for all of the short fetch one-hour records.
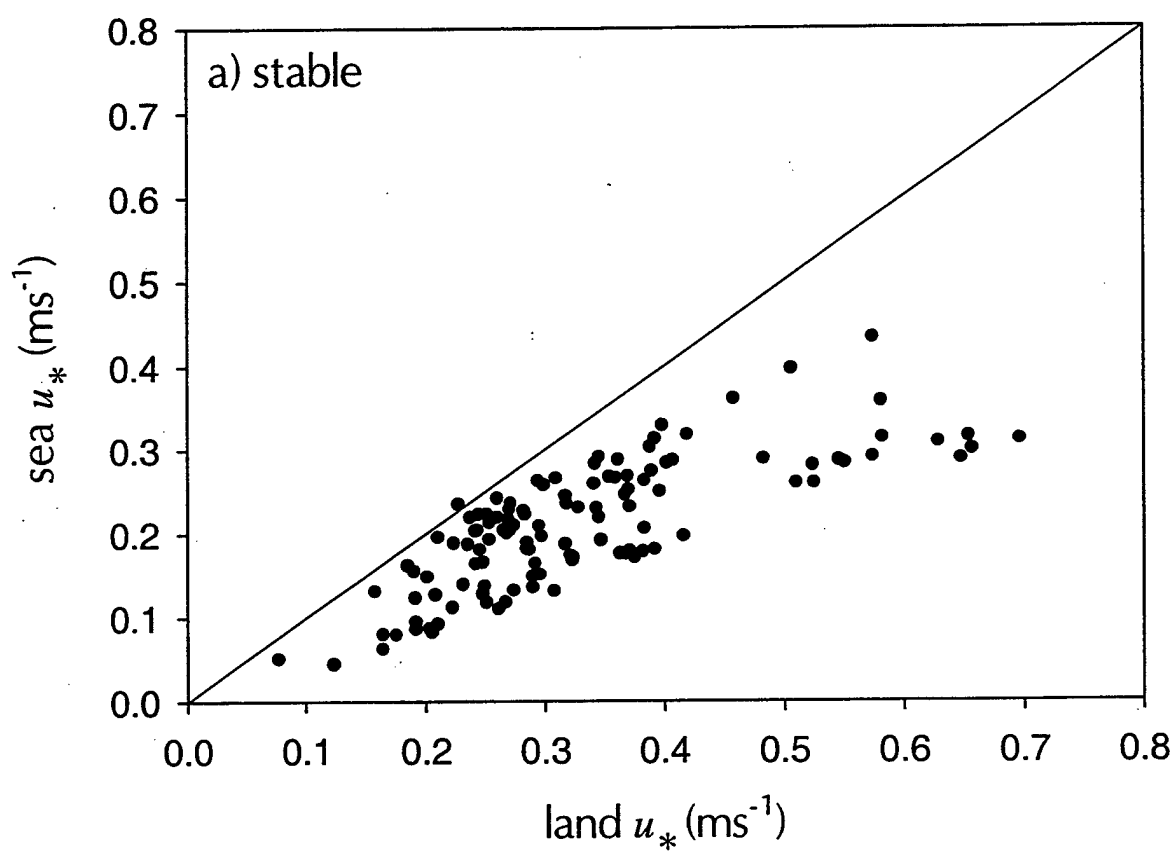
Figure 3a. Relationship of the offshore friction velocity (ms^{-1}) to the land-mast value for stable conditions.
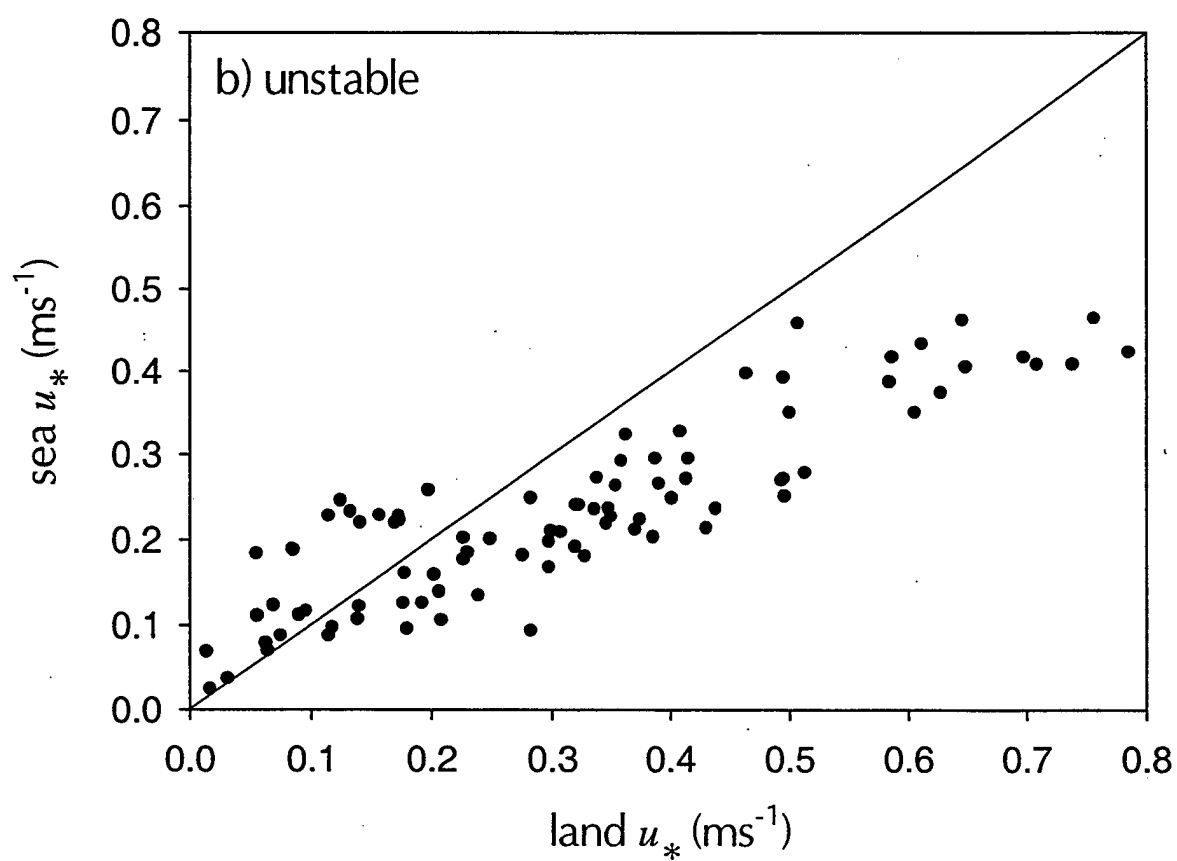
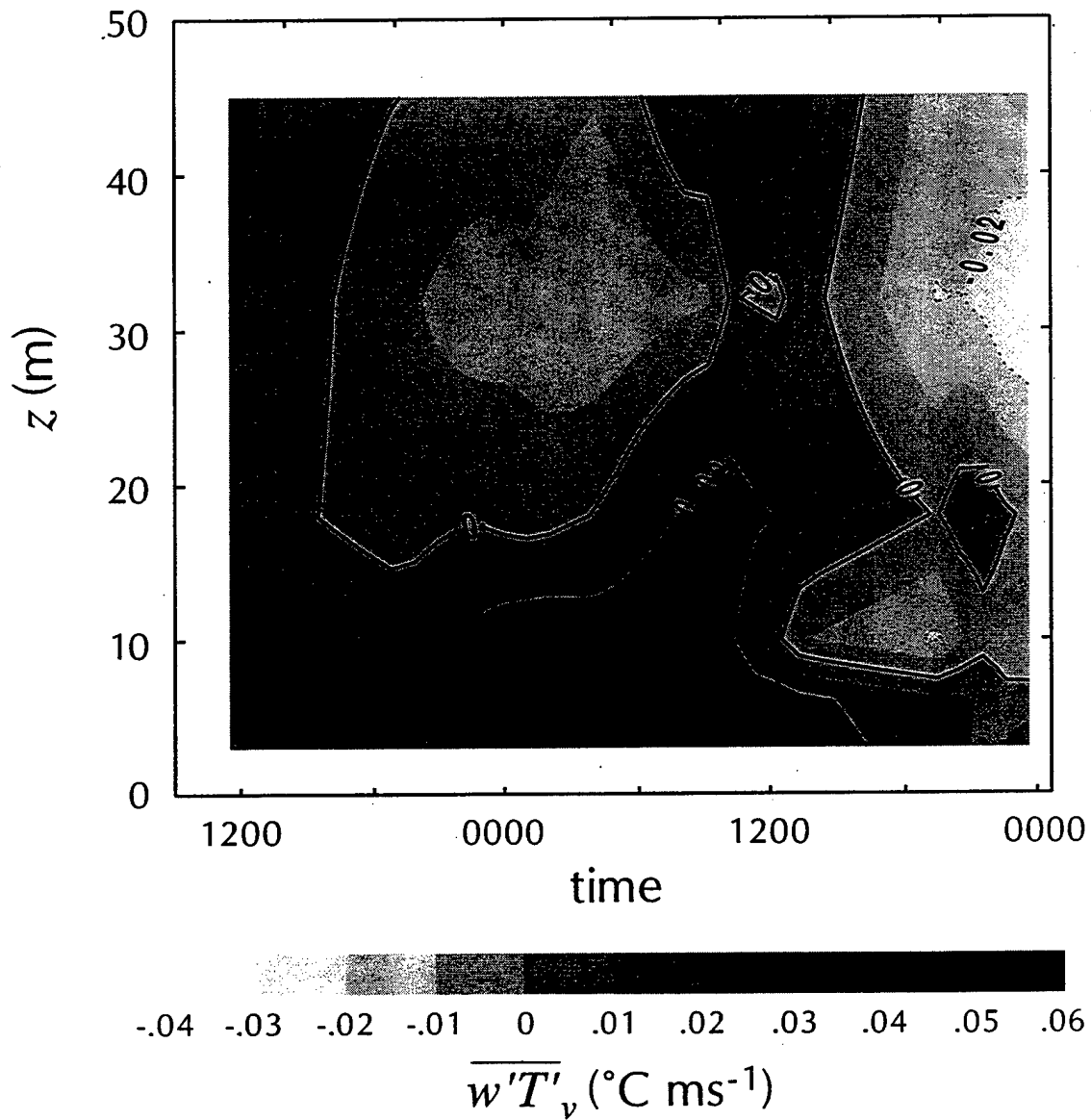Figure 3b. Relationship of the offshore friction velocity (ms^{-1}) to the land-mast value for unstable conditions.

Figure 4. Time-height cross-section for unstable case UI for the buoyancy flux ($°Cms^{-1}$) where darker areas correspond to upward buoyancy flux. Times are GMT which is one hour behind local solar time.

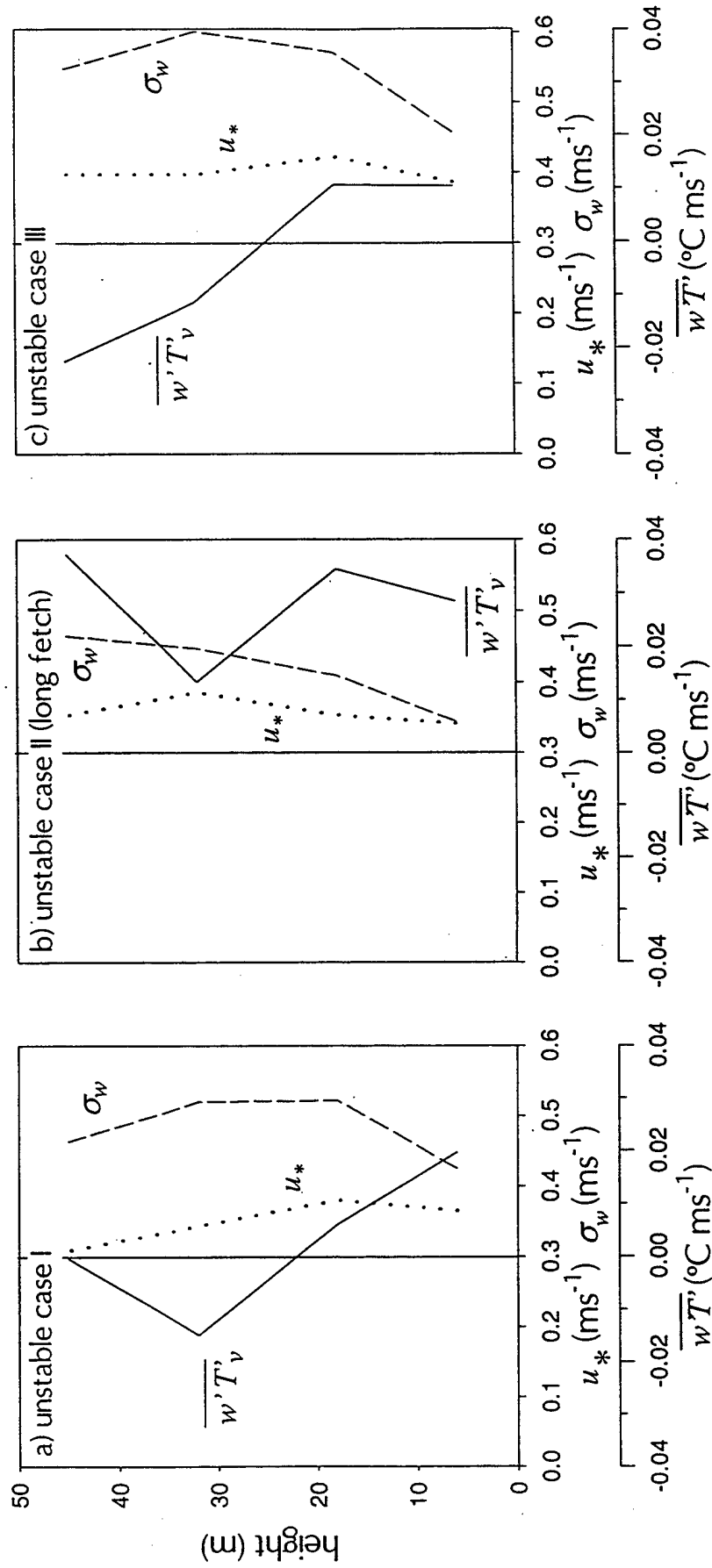Figure 5a-c. Vertical profiles of the friction velocity (ms^{-1}), buoyancy flux ($°Cms^{-1}$) and σ_w (m^2s^{-2}) for the three unstable cases.
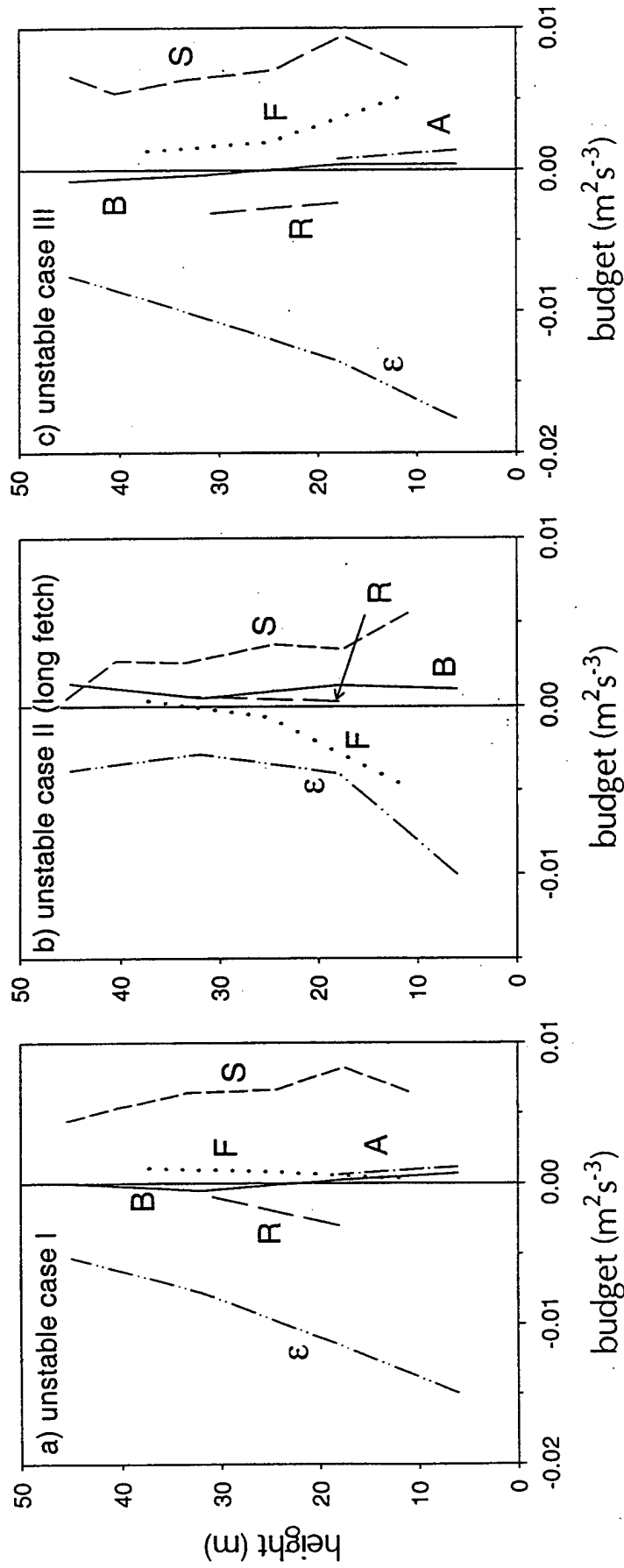
Figure 6a-c. The turbulence energy budget ($m^2 s^{-3}$) for the unstable cases. A is the advection term, ϵ the dissipation, S the shear-generation term, F the vertical divergence of the flux of the turbulence energy, B the buoyancy-generation term and R, the residual.
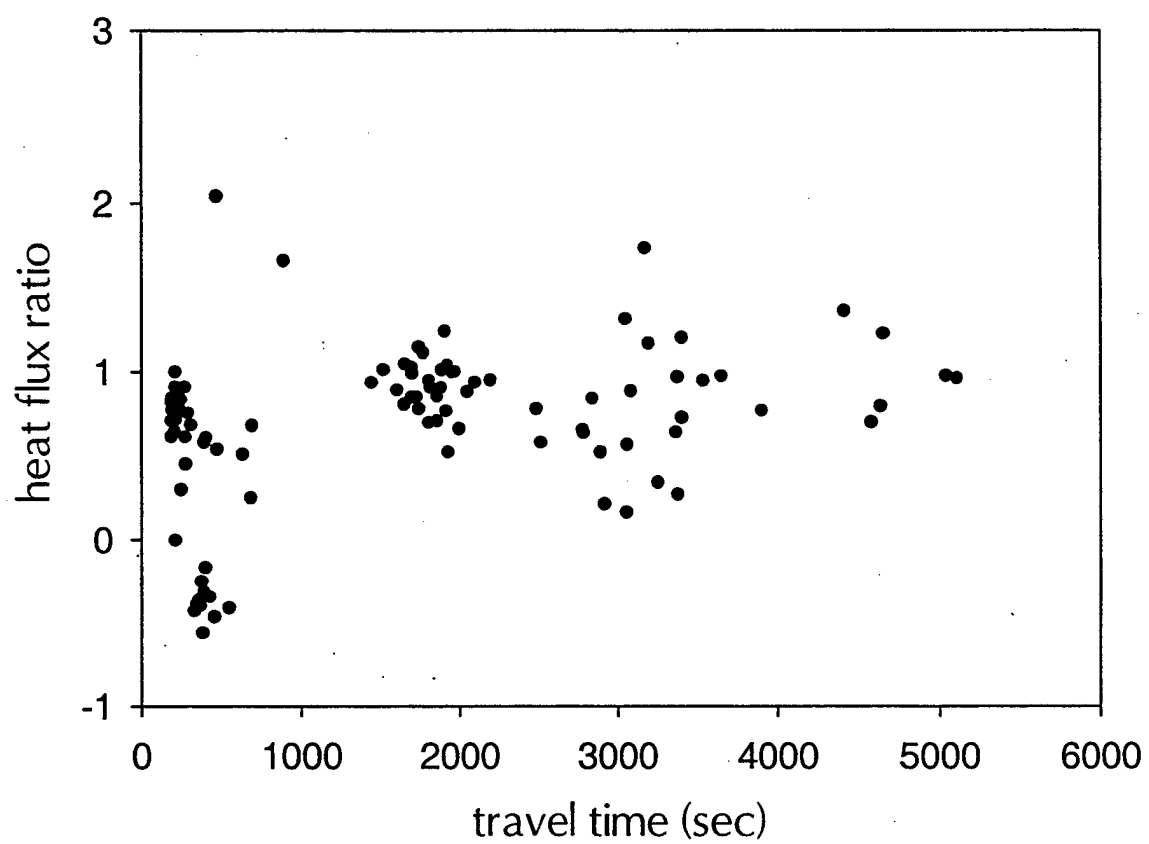
Figure 7. Buoyancy flux ratio (Eq. 3) as a function of travel time for all of the unstable records ($z/L < -0.1$) .

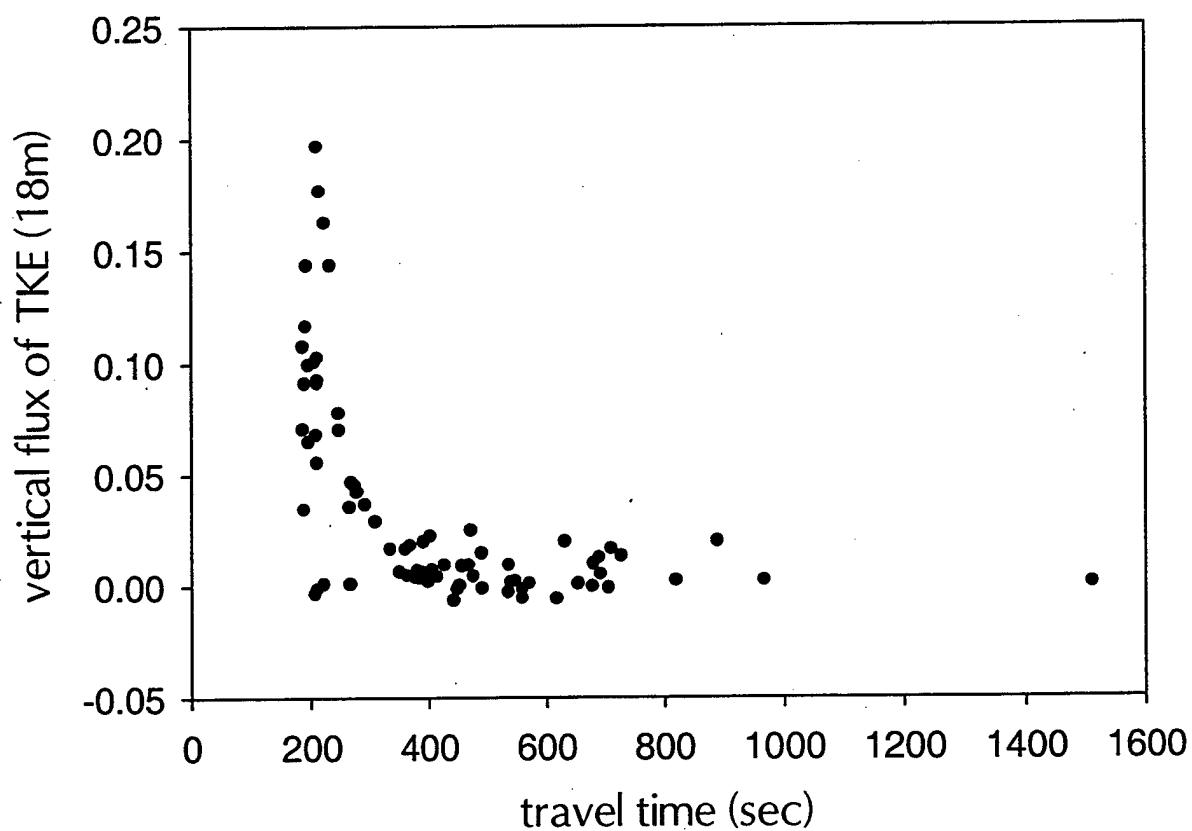Figure 8. The dependence of the vertical flux of turbulence energy $(m^3 s^{-3})$ at 18 m on travel time for all of the one-hour records with fetch values less than 5 km for unstable conditions $(z/L < -0.1)$.

33

Figure 9. Time-height cross-section of the buoyancy flux ($°Cms^{-1}$) for stable case SI where lighter areas correspond to stronger downward buoyancy flux. Times are GMT which is one hour behind local solar time.

Figure 10. Vertical profiles of the friction velocity (ms^{-1}), buoyancy flux $(°Cms^{-1})$ and σ_w (ms^{-1}) for the three stable cases (a, c, d) and for a one-hour subperiod during case SI where fluxes are very weak (panel b).

Figure 11. The turbulence energy budget ($10^{-3} m^2 s^{-3}$) for the three stable
Cases (a-c). A is the advection term, ϵ the dissipation, S the shear- genera-
tion term, F the vertical divergence of the flux of the turbulence energy, B
the buoyancy-generation term and R, the residual.

Figure 12. The stress ratio (Eq. 2) as a function of travel time for all of the one-hour records with stable conditions ($z/L > 0.1$).

Figure 13. The dependence of the vertical flux of turbulence energy $(m^3 s^{-3})$ at 18 m on travel time for all of the one-hour records with stable conditions $(z/L > 0.1)$.

Figure 14. The relationship between the turbulence energy flux $(m^3 s^{-3})$ at 18 m and the momentum flux ratio for stable conditions based on bin-averaged values computed from the one-hour records. Also shown are standard error bars.

THE COASTAL ZONE

LARRY MAHRT
College of Oceanic and Atmospheric Sciences
Oregon State University
Corvallis, OR 97331, USA

10.1 Introduction

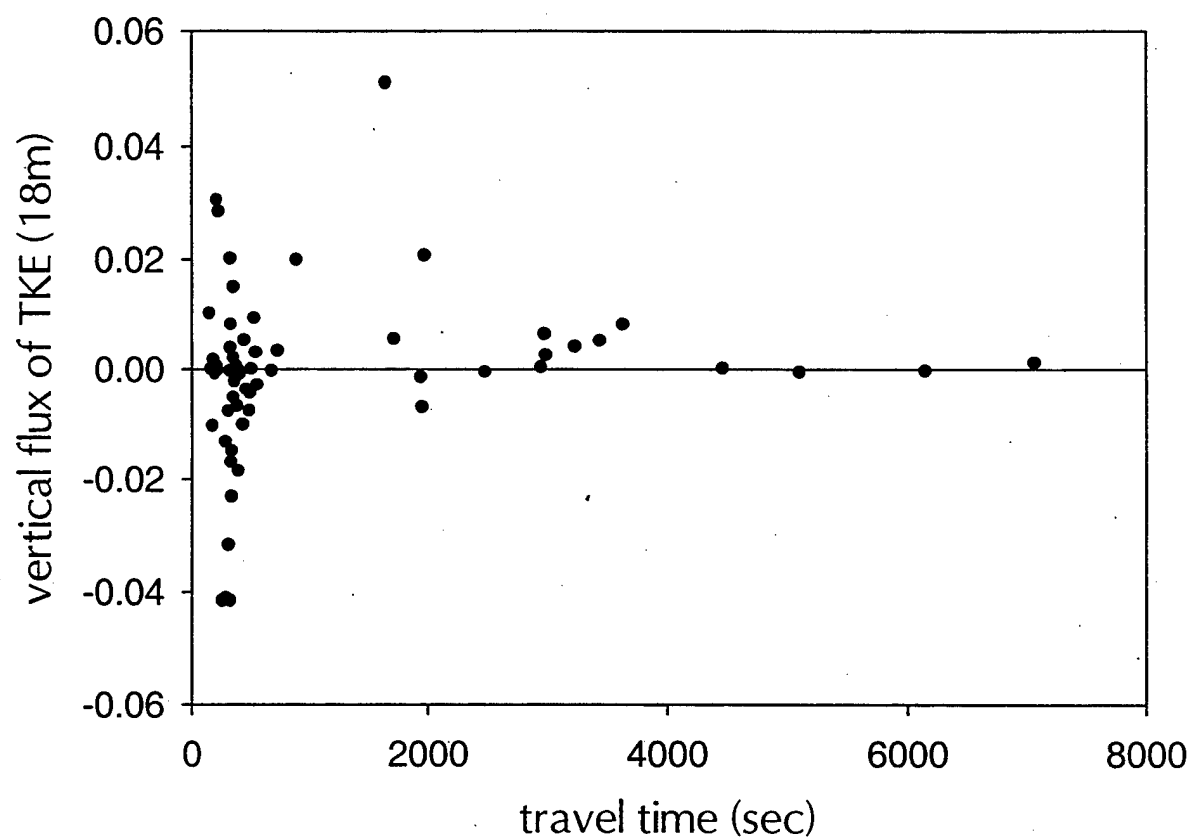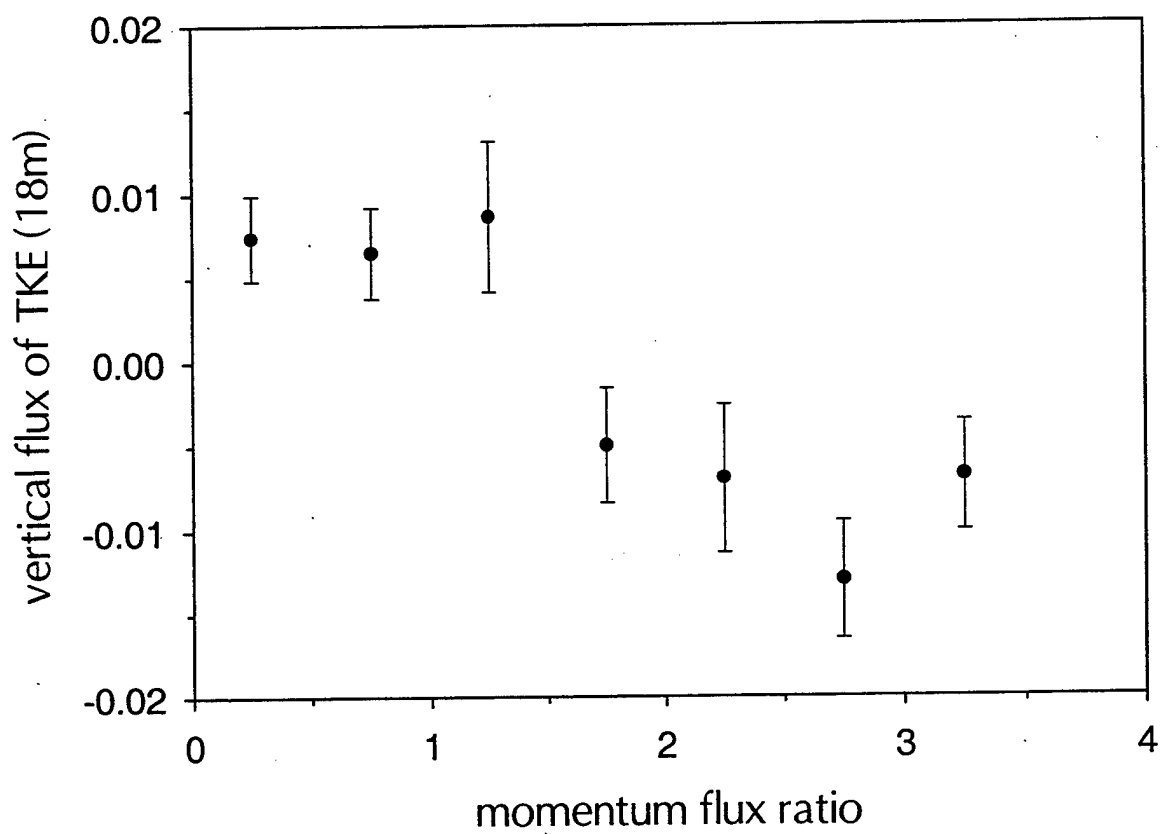The coastal zone is of considerable practical importance since it is a region of intensive human activity and rich in biological activity, compared to the open ocean. At the same time, the spatial variation of the atmospheric surface flow and the surface wave field are complex and both are often in nonequilbrium. Formulations of surface stress must include the influence of developing wave state and shoaling (Section 3). Growing waves occur with offshore flow and with time-varying wind fields, often induced by diurnal variation of the heat flux discontinuity at the coastal interface (Section 5). Current formulations of the surface flux may perform poorly in developing internal boundary layers in offshore flow (Section 4). Difficulties with formulation of surface fluxes in the coastal zone is a major topic of this chapter (Sections 2-3). Offshore flow must adjust to smaller surface roughness and different surface heat flux over the sea. The modelling problem is particularly difficult with offshore flow of warm air over a cool water surface (Section 4). The development of stratus and other cloud regimes in the coastal zone is beyond the scope of this survey. This chapter will assume familiarity with previous reviews found in Donelan (1990) and Geernaert (1990).

10.2 Formulation of surface fluxes

The surface stress, heat flux and moisture flux are formulated through the bulk formulas:

$$(\overline{w'u'}^2 + \overline{w'v'}^2)^{1/2} = C_d \overline{u}^2 \qquad (10\text{-}1)$$

$$\overline{w'\theta'} = C_h \overline{u} [\theta_o - \overline{\theta}]$$

(10-2)

$$\overline{w'q'} = C_q \overline{u} [q_o - \overline{q}]$$

(10-3)

where C_d is the drag coefficient, C_h is the transfer coefficient for heat, C_q is the transfer coefficient for moisture, z is the observational height, θ_o and q_o are surface aerodynamic values of the potential temperature and specific humidity, to be defined below, and $\overline{u}$ is the speed of the vector averaged wind where the x-coordinate has been rotated into the direction of the mean wind. Similar bulk formulations can be written for turbulent transfer of other scalars although definition of the aerodynamic surface quantities becomes problematic (Sun et al. 1998a). Numerous variations of the bulk formula are used where the vector averaged speed is replaced by the averaged instantaneous speed, the total stress is replaced by the stress in the along-wind direction, or the current velocity is removed from the wind (see Mahrt et al. 1998). Since the stress, wind and wave propagation directions may be systematically different (Geernaert 1990; Rieder et al. 1994; Rieder 1996), omission of the cross wind stress seems inadvisable even though this component can be characterized by large flux sampling errors.

In the case of weak winds, the precise definition of the velocity used in the bulk formula becomes important. This velocity scale has been generalized to include the influence of "large convective eddies" (Beljaars 1995; Fairall et al. 1996; Grachev et al. 1998) or mesoscale motions which are on smaller scales than the spatial or grid-averaging scale (Mahrt, Sun 1995; Vickers, Esbensen 1998). Resolving this problem is made difficult by severe flux sampling errors in the weak wind case (Mahrt et al. 1996) which can be reduced only with long stationary records. With weak winds and swell, the momentum flux may even be transported from the waves to the atmosphere (e.g. Smedman et al. 1994).

The simplest formulation of the surface stress specifies the neutral drag coefficient to be constant or a function of wind speed but independent of wave state (see studies surveyed in Geernaert, 1990). The transfer coefficient for heat is often specified to be constant where θ_o is equated to the surface radiation surface temperature of the water or the near-surface water temperature and q_o is specified to be the saturation specific humidity evaluated at the value of the surface temperature. The appealing simplicity of this approach meets the demand of economy required in some large scale models.

However, in the coastal zone, stability strongly influences the transfer coefficients. One might expect stability $-z/L$ to be smaller over water than over land since surface heat fluxes are typically smaller over water than over land, where L is the Obukhov length

$$L \equiv \frac{u_*^3}{\kappa z (g/\theta_v) \overline{w'\theta_v'}}$$

(10-4)

where u_* is the surface friction velocity (square root of the surface stress magnitude) and κ is the von Karman constant. However, the shear stress is also weaker over the sea than over land due to small surface roughness so that the stability $-z/L$ can significantly influence the transfer coefficients even without strong surface buoyancy flux. As a

41

result, stability may strongly influence the flux-gradient relationship in the coastal zone. To include the influence of stability on the drag coefficient and transfer coefficients, Monin-Obukhov similarity theory (Monin, Obukhov 1954) is applied by either:

1) using similarity theory to reduce the drag and transfer coefficients to their equivalent neutral values (Section 10.2.2) and relating the neutral values to the wind speed and wave state or

2) explicitly applying Monin-Obukhov similarity theory and relating the roughness length to wave state (Section 10.3.2).

10.2.1 MONIN-OBUKHOV SIMILARITY THEORY

Monin-Obukhov similarity theory provides a model for the flux-gradient relationship in the surface layer, above the wave boundary layer (Figure 10.1). In the surface layer, the flux-gradient relationship is assumed to be independent of the wave state and a universal function of only z/L. This flux-gradient relationship is posed in terms of the nondimensional vertical gradient

$$(z/L) \equiv \frac{(\partial \bar{\theta}/\partial z)(\kappa z u_*)}{\overline{w'\theta'}(z)} \tag{10-5}$$

$$\phi_m(z/L) \equiv \frac{(\partial \bar{u}/\partial z)(\kappa z)}{u_*} \tag{10-6}$$

which have been empirically fitted to dependencies on z/L (Högström 1988). The nondimensional gradient ϕ can be interpreted as the inverse of the mixing efficiency. The transfer of moisture and other scalars are often assumed to follow the same dependence as that for heat. This interpretive survey will concentrate on transfer of heat and momentum as examples.

The surface drag coefficient and transfer coefficient for heat are estimated by vertically integrating the ϕ functions downward to the surface roughness lengths in which case one can derive:

$$C_d = [\frac{\kappa}{ln(z/z_o) - \psi_m}]^2 \tag{10-7}$$

$$C_h = [\frac{\kappa}{ln(z/z_o) - \psi_m}][\frac{\kappa}{ln(z/z_{oh}) - \psi_h}] \tag{10-8}$$

where z_o and z_{oh} are the roughness lengths for momentum and heat, respectively, and ψ and ψ_h are the integrated analytical forms of the nondimensional gradients for momentum and heat, ϕ_m (z/L) and ϕ_h (z/L). This vertical integration (Paulson, 1970) requires that the fluxes and the wind direction are approximately independent of height and requires additional mathematical approximations (Enriquez, Friehe 1997). The nondimensional vertical gradients, ϕ_m (z/L) and ϕ_h (z/L), have not been extensively evaluated over the sea. Recently, Højstrup (1998) found that for onshore flow in the coastal zone, the land-based stability dependence for ϕ_m (z/L) approximated the observed

42

values of ϕ_m although the scatter was large. Conflicting evidence is noted in the next subsection.

Note that Monin-Obukhov similarity theory does not describe the actual flux-gradient relationship below the surface layer in the wave boundary layer. The extrapolated wind profile described by similarity theory vanishes at the roughness height z_o instead of at the surface. As a result, the extrapolated and actual wind profiles in the wave boundary layer are not expected to be the same. The extrapolated profile of potential temperature is also expected to be different from the actual profile in the wave boundary layer, and reaches the "aerodynamic" surface temperature at the roughness height for heat, z_{ot}. Both the aerodynamic surface temperature θ_o and z_{ot} are unknown. Specifying θ_o to be the surface radiation temperature or near-surface water temperature redefines the roughness height for heat z_{ot}. Over the open ocean, the thermal roughness height is normally related to the roughness length for momentum (Lui et al. 1979). In the coastal zone, Mahrt et al. (1998) find little relationship between z_{ot} and z_o where z_{ot} appears to be strongly influenced by development of internal boundary layers while z_o is more influenced by wave state. Both the physical meaning of the roughness height for heat and its dependence on other parameters remain elusive, especially in the coastal zone.
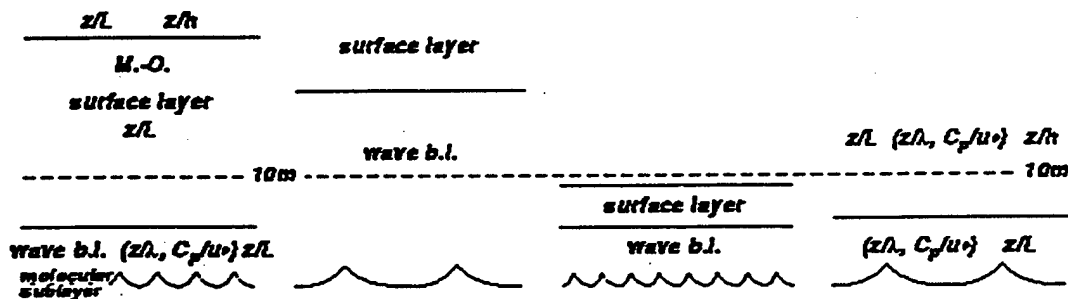
Figure 10.1 Idealized layering of the lower boundary layer. Using 10 m as a reference height, the first scenario shows the ideal case where Monin-Obukhov similarity theory applies. In the second example, the reference level is in the wave boundary layer and wave length scales are required to describe the local flux-gradient relationship. In the third example, the reference level is above the surface layer and bulk boundary-layer scaling is required. In the fourth example, the influence of the boundary-layer depth extends downward to the wave boundary layer and the conditions for Monin-Obukhov similarity theory are not met at any level.

10.2.2 REDUCING TO NEUTRAL

To eliminate the influence of stability, the drag coefficient and transfer coefficients are sometimes reduced to their neutral values (Deardorff 1968). This procedure attempts to eliminate the influence of stability so that the neutral drag and transfer coefficients can be studied as a function of wave state and wind speed. The reduction of the transfer coefficient to neutral conditions using Monin-Obukhov similarity theory must impose restrictions on the roughness length such as Charnock's relationship with constant coefficient (Geernaert, Katsaros 1986; Geernaert 1990). Smith (1980, Figure 13),

43

Geernaert (1988) and Mahrt et al. (1996) find that the reduction of the drag coefficient to neutral values does not completely remove the influence of stability although it is not clear if the stability functions $\phi_m(z/L)$ and $\phi_h(z/L)$ themselves are incorrect, measurement errors are large or influences not included in the Obukhov length are large.

10.2.3 WAVE BOUNDARY LAYER

The wave boundary layer is the layer adjacent to the wave surface, but above the very thin laminar sublayer at the surface (Figure 10.1). In the wave boundary layer, part of the atmospheric transporting motions are directly induced by the waves and associated perturbation pressure field in the air (Chalikov, Belevich 1993; Hare et al. 1997). The depth of the wave boundary layer is thought to scale with the surface wavelength (Chalikov, Belevich 1993). Multiple wave boundary layers associated with wind driven waves and swell may coexist. However, the transport by eddies in phase with the swell may be small since the swell are characterized by small slopes. In the wave boundary layer, Monin-Obukhov similarity theory does not describe the local flux-gradient relationship which depends partly on the amplitude and wavelength of the dominant surface wave (Large et al. 1995). Apparently, the profile functions, ϕ_m and ϕ_h depend on z/λ as well as z/L (or equivalently z/L and λ/L) where λ is a dominant wave dimension, either wave length or wave height.

Consequently, Monin-Obukhov similarity theory must be applied in the surface layer above the wave boundary layer, along with specified roughness lengths, in order to predict the surface fluxes. Analogously, over land, Monin-Obukhov similarity must be applied in the surface layer above the roughness sublayer to predict surface fluxes. Eqs. (10-1)-(10-2) correctly predict surfaces fluxes using Monin-Obukhov similarity theory for the drag and transfer coefficients (Eqs. (10-7)-(10-8)) only if the roughness lengths can be appropriately specified.

There are two fundamental differences between the flux-gradient relationship over the sea and that over land:

1) In the roughness sublayer over land, the time-averaged flow may vary horizontally on the scale of the roughness elements due to semi-stationary pressure perturbations anchored to individual roughness elements. Over the sea, the roughness elements (surface waves) propagate so that such microscale spatial variability of the time-averaged flow does not normally exist.

2) Over the sea, the roughness length for momentum varies substantially with wave state. Over land, z_0 is normally considered to be independent of time for a given wind direction.

However, there is no obvious reason why these differences would reduce the applicability of Monin-Obukhov similarity theory over the sea, provided that the appropriate surface roughness lengths can be specified in a reasonably simple fashion. In fact, Monin-Obukhov similarity theory is more likely less applicable over land where the required assumption of homogeneity is normally violated to some degree. Even over apparently homogeneous land surfaces, microscale variations of soil moisture can influence local eddy structure. Nonetheless, there are special processes in the coastal zone which violate assumptions required for Monin-Obukhov similarity theory.

10.2.4 THEORY BREAKDOWN IN THE COASTAL ZONE

Existing similarity theory may break down in the coastal zone due to the following influences:

1. Strong horizontal advection leads to significant vertical divergence of the flux. For example with steady-state temperature advection, $\bar{u}\partial\bar{\theta}/\partial x \approx -\partial\overline{w'\theta'}/\partial z$. Then the assumption of height-independent fluxes is not a good approximation and the vertical integration of the nondimensional gradients, ϕ, to obtain the stability corrections for the transfer coefficients, ψ (Eqs. (10-7)-(10-8)), is not valid.

2. If the flux decreases to small values at the top of the thin internal boundary layers in offshore flow, then the vertical divergence of the flux is large. As a result, standard observational levels, such as 10 m, may be above the thin surface layer where one can neglect the height-dependence of the flux (Figure 10.1). The depth of the surface layer is bounded by some small fraction of the boundary-layer depth, sometimes chosen as 10%, such that the height-dependence of the flux can be neglected in the surface layer. For example, in an internal boundary layer of 50 m depth, the surface layer would theoretically be less than 5 m depth. Note that influences 1) and 2) are not independent.

3. With offshore flow of warm air over cold water, the turbulence may be a top-down process where the primary source of turbulence is above the surface inversion (Section 10.4.2). It is not clear if Monin-Obukhov similarity theory is valid in this "upside-down boundary layer".

4. The turbulence in offshore flow does not establish equilibrium with the rapidly evolving mean flow immediately downstream from the coast.

5. With cold (warm) air advection in offshore flow, the wind vector tends to rotate to the right (left) with height and the surface stress vector is directed to the right (left) of the surface wind vector (Geernaert 1988). Integration of Monin-Obukhov similarity theory assumes that the wind and stress vectors are aligned and their height-dependence can be neglected.

6. It may be that Monin-Obukhov similarity theory is valid but the stability functions, ϕ_m and ϕ_h, are not correctly calibrated.

If the internal boundary layer is sufficiently thin, yet the wave boundary layer is deep (large surface wavelength), the surface layer may be "squeezed out" as postulated by Mahrt et al. (1998) and shown in Figure 10.1 (right hand side). That is, there is no layer where the flux-gradient relationship depends only on z/L and the influence of boundary-layer depth, h, and surface wave dimension λ must be included as additional scaling variables. Grant (1992) suggests that $\phi(z/L)$ for the near neutral boundary layer should be generalized to be of the form $\phi(z/h, h/L, u_*/fh)$ where f is the Coriolis parameter. Khanna and Brasseur (1997) consider the form $\phi(z/L, h/L)$. In the LES results of Khanna and Brasseur (1997), the nondimensional shear decreases above the surface layer, as is also observed by Smedman and Johannson (1997) in shallow offshore boundary layers. With a well-mixed interior of the boundary layer, the vertical gradient decreases faster with height than the flux. Mahrt et al. (1998) find that the thin depth of observed offshore internal boundary layers suppresses heat transfer by the large convective eddies which in turn implies that ϕ_h is larger than predicted by Monin-Obukhov similarity theory and depends on z/h.

45

Davidson (1974) found that ψ_m and the drag coefficient are both a function of stability and wave age and that these dependencies are difficult to sort out since the wave age and stability were significantly correlated for their data. Bergström and Smedman (1995) examined the functional dependence ϕ_m $(z/L, C_p/u_*)$ but found that the relationship to wave state was statistically insignificant, although they note that their data represents a relatively narrow range of conditions. Here, C_p is the phase speed of the dominant wave.

Since for offshore flow, there may be no level where ϕ_m is a function of only z/L, it is useful to consider a more general formulation such as

$$\phi_m \equiv \frac{(\partial \overline{u}/\partial z)\ (\kappa z)}{u_*} = f(z/L,\ z/\lambda,\ C_p/u_*, z/h) \tag{10-9}$$

Note that the arguments z/L, z/λ, C_p/u_*, z/h are not independent. Large et al. (1995) prefer to partition the nondimensional shear into two functions, the traditional ϕ_m (z/L) and a modifying function $\chi(z/\lambda)$, as also pursued by Vickers and Mahrt (1998). Specific forms of Eq. (10-9) based on actual eddy correlation data have not been established.

Monin-Obukhov similarity theory is also complicated by the possible dependence of the von Karmen "constant" on the roughness Reynolds number, Re_* defined as $u_* z_o/\nu$. Generally, $\kappa(Re^*)$ is found to decrease with increasing roughness Reynolds number (Tennekes, 1968). With this possibility, evaluation of $\phi_m(z/L)$ from data using Eq. (10-6) results in two unknowns, $\kappa(Re_*)$ and $\phi_m(z/L)$. Oncley et al. (1996), Miller et al. (1997) and others eliminate $\phi_m(z/L)$ as an unknown by considering near neutral cases and assuming $\phi_m(z/L) = 1$. Then, $\kappa(Re_*)$ is estimated as

$$\kappa(Re_*) = \frac{u_*}{z \partial \overline{u}/\partial z} \tag{10-10}$$

Since both Re_* and z/L depend on u_*, their dependencies are difficult to isolate from data. For example, failure to include the dependence $\kappa(Re_*)$, if important, would alter the value of $\phi_m(z/L)$ computed from data. Conversely, if influences of z/L are not completely negligible, such influences could create an artificial dependence of κ on the roughness Reynolds number. The problem becomes even more complex if the nondimensional shear is dependent on wave age (Eq. (10-9) since the wave age also depends on u_*.

10.3 Wave state

In the coastal zone, the stress is influenced by shoaling processes and wave breaking as waves propagate into shallow water (Smith 1980; Freilich et al. 1990). For waves propagating toward the shore, wave modification first occurs when the depth of the water shallows to be about 1/4 of the dominate wavelength. At this point, the wave amplitude begins to increase, the wavelength and propagation speed begin to decrease and the spectral characteristics change. Closer to the shore where the depth becomes less than one wave height, dramatic wave steepening and breaking occur (Thornton,

Guza 1982, 1983; Holman, Sallenger 1985; Holland et al. 1995). Irregularities of the bottom topography along the coast and wave refraction lead to irregularities in the surface wave field along the coast (Munk, Traylor 1947).

Information on wave state is necessary for modelling surface stress in the coastal zone. This information is included at three levels of approximation: 1) relating the drag coefficient or roughness length to the wave age is the most common approach (Section 10.3.1); 2) relating the stress to different frequency bands of the wave field, such as swell and wind-driven modes, is more complete but requires more information on the wave field (Section 10.3.2) and 3) modelling the wave age in terms of fetch is less accurate but is useful when explicit information on wave state is not available (Section 10.3.3).

10.3.1 WAVE AGE DEPENDENCE

With offshore flow, the wind driven waves are growing in the downstream direction which become evident seaward of the inner shoaling zone. A number of investigators have documented that the stress is greater over a young and developing wave field than over an older wave field, which is in near-equilibrium with the wind field (e.g. Donelan 1990; Kitaigorodskii 1973; Nordeng 1991; Geernaert et al. 1987, 1988; Donelan 1990; Maat et al 1991). At least two mechanisms contribute to the dependence of stress on wave age: 1) younger waves propagate with slower phase speed relative to the wind and thus provide greater bulk shear, and 2) younger growing waves may be steeper, which can lead to enhanced flow separation from individual wave crests. Younger developing waves occur with changing wind vector as well as with fetch limited off-shore flow.

Previous studies suggest that the drag coefficient is a maximum for a wave age of 10 (Nordeng 1991) and 7 (Geernaert, Smith 1996). Kitaigorodskii et al. (1995) similarly find maximum roughness length at an intermediate wave age. In the absence of swell (inland seas), the drag coefficient may be immeasurably small immediately downstream from the shore where waves have not yet developed or are very small amplitude. The subsequent wave growth in the downstream direction leads to larger stress, as sketched in Figure 10.2. The wave growth in the downwind direction can be further enhanced by acceleration of the offshore wind resulting from the smaller surface roughness over the sea than over land. However, at some point, the increasing phase speed of the waves and resulting reduction of the relative flow of the wind over the waves becomes more important than the effect of increasing wave amplitude and any increase of slope. Then the stress and drag coefficient begin to decrease further downstream. Consequently, the drag coefficient reaches a maximum at an intermediate wave age and decreases with further increase of wave age. Similar effects appear in the model of Hansen and Larsen (1997) where the Charnock constant reaches a maximum at a wave age of about 5. Most observations occur at wave ages greater than this intermediate wave age so that the drag coefficient is generally considered to decrease with increasing wave age, as in the studies surveyed below.

Vickers and Mahrt (1997) find that onshore flow with shoaling, can also occur with small values of the wave age. The shoaling reduces the wave phase speed and decreases the numerical value of the wave age. Consequently, shoaling complicates the physical interpretation of wave age in the coastal zone. The corresponding drag coefficient may increase by more than 50% with such shoaling. As a result, Kitaigorodskii et al. (1995) related the momentum roughness length to wave breaking characteristics. Mahrt et al. (1998) found no detectable increase in the transfer coefficients for heat and moisture

with wave breaking. Relative insensitivity of the transfer coefficients for heat and moisture to wave state and wind speed was also found in Smith (1980), Makin and Mastenbroek (1996) and references therein.

Since the stress appears to be related to the relative flow of the air with respect to the phase speed of the dominate waves (Kitaigorodskii 1973), one is tempted to re-define the drag coefficient in terms of the relative flow $\bar{u} - C_p$ where C_p is ideally the component of the phase speed of the dominant wave in the wind direction. However, the stress does not necessarily vanish as $\bar{u} - C_p$ approaches zero, since waves with frequencies different from the dominant wave contribute to the stress and propagate with different phase velocities. For example, with mature waves, much of the stress is thought to be associated with capillary waves and therefore not related to the phase speed of the dominant waves. As a result of the stress from capillary waves, the alternate drag coefficient, defined as the ratio of the stress to $\bar{u} - C_p$, approaches infinity as $\bar{u} - C_p$ approaches zero.

However the traditional drag coefficient computed from (Eq. (10.1)) may be better related to $\bar{u} - C_p$ than $\bar{u}$ alone. To examine this problem, we computed the drag coefficient from eddy correlation data collected at a tower 2 km off the Danish coast in the Risø Air Sea Experiment (RASEX, Barthelmie 1994; Højstrup et al. 1994; Mahrt et al. 1996). The drag coefficient reaches a minimum value near $\bar{u} - C_p = 0$ m/s and a regression model of the drag coefficient based on $\bar{u} - C_p$ explains more variance than that based on $\bar{u}$. However, the drag coefficient is more closely related to wave age than $\bar{u} - C_p$ probably because wave age implicitly accounts for the relative flow over the waves as well as implicitly includes the effect of wave amplitude and steepness.

Geernaert et al. (1987) proposed a model of the dependence of the neutral drag coefficient on wave age of the form

$$C_{dn} = b\,(C_p/u_*)^{-2/3} \tag{10-11}$$

where b is on the order of 10^{-2}. Vickers and Mahrt (1997) found that this model performed well in the coastal zone even after accounting for the role of self-correlation. They found that -2/3 was indeed the best fit to the exponent while the best fit value of b was approximately 7×10^{-3}.

The drag coefficient can also be computed directly from Monin-Obukhov similarity theory in which case the roughness length is a function of wave state. The Charnock (1955) prediction of the roughness length, 0.019 (u_*^2/g), is often generalized to include a dependence on inverse wave age (Toba, Koga 1986; Maat et al. 1991; Donelan 1990; Smith et al. 1992). If we also incorporate the smooth flow contribution to the roughness length (Donelan 1990; Fairall et al. 1996), then the full relationship is of the form

$$z_o = K\,(u_*^2/g)\,(u_*/C_p)^p + 0.11\nu/u_* \tag{10-12}$$

48

offshore flow and no swell

unstable case

capping inversion

decaying residual turbulence

1 km –

↑

z

cool ⟹

Internal boundary layer

stress

↑

stress

| 0 | 5 | 10 | 15 | 20 | 25 |

$C_p/u_* \longrightarrow$

stable case

100 m –

↑

z

decaying turbulence

⟹ **jet**

warm ⟹

turbulent recoupling

↑

stress

stress

decoupling
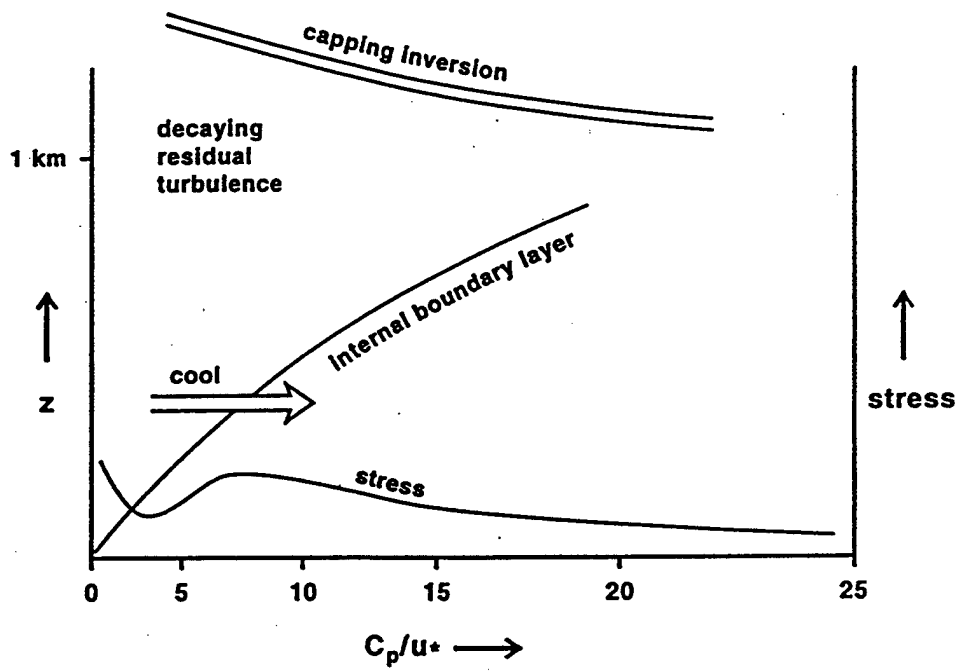
distance from shore ⟶
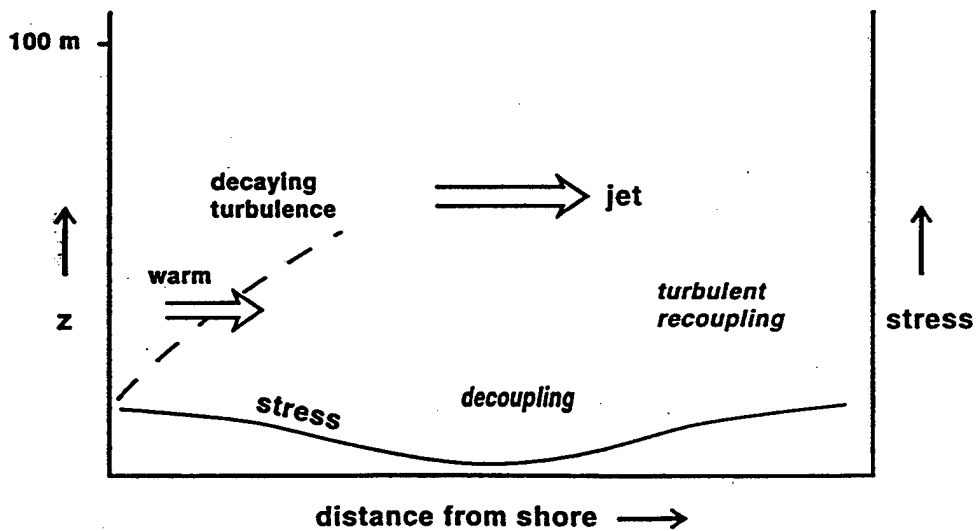
Figure 10.2 Plausible schematic evolution of the internal boundary layer for unstable and very stable offshore flows. In the unstable case, the x-axis can also be qualitatively interpreted as the downstream distance.

49

where typically $K = 0.48$ and $p = 1$ (Smith et al. 1992), and v is the viscosity of air. Wu (1968) suggested an additional term due to parameterized surface tension which was recently applied in Alam and Curry (1997).

Alternatively, the model of Kitaigorodskii (1970) is of the form,

$$z_o = K \sigma \exp(-\kappa C_p / u_*) \qquad (10\text{-}13)$$

where $K = 0.3$, σ is the root mean square amplitude of the waves and κ is von Karman's constant. The Kitaigorodskii representation follows from explicitly including the shear between the wind and the wave velocity and integrating over the full wave spectrum.

A significant fraction of the variance explained by these models is due to self-correlation since the drag coefficient and roughness length are both defined in terms of the surface friction velocity and are both formulated in terms of the surface friction velocity on the right hand sides of Eqs. (10-11)-(10-13) (e.g. Smith et al. 1992; Vickers, Mahrt 1997). To avoid self-correlation, the wave age is sometimes expressed in terms of $C_p / \bar{u}$ where $\bar{u}$ is the wind speed at a standard level or at a fixed height relative to the surface wavelength (Donelan 1990).

The roughness length is sometimes related to other characteristics of the wave field. For example, Anctil and Donelan (1996) relate the spatial variation of the roughness length in the shoaling zone to the wave age, root mean squared displacement height of the waves and root mean square wave slope. Kitaigorodskii et al. (1995) relate the roughness length to the effective wave height.

10.3.2 MULTI-MODE MODELS

The need for models based on multiple wave modes is motivated by the fact that the wind driven waves and swell often propagate in different directions. The swell modifies the stress direction so that it may be different from the wind direction (Geernaert et al. 1995). A family of parameterizations of the roughness length as a weighted integral of the wave spectra have been formed from the original framework of Kitaigorodskii (1973) as in Hansen and Larsen (1997). See also Chalikov and Belevich (1993) and papers surveyed in Geernaert (1990). Kitaigorodskii et al. (1995) focus on the width of the wave dissipation regime in an effort to understand the variability of surface roughness. The most complete description of the wave field can be obtained from explicit wave models such as the "WAM" model (WAMDI group, 1988). The advantage of relating the surface roughness to the wave spectra avoids the parameterized coupling between the surface roughness and with the wind field or stress field itself that occurs with the approaches in the preceding section. At the same time, complete information on the full wave spectra is normally not available.

Simplified models which allow some information of differences between wave modes include the two band model of Donelan (1982) which distinguishes between the drag associated with short and long waves. Vickers and Mahrt (1997) develop a crude indicator of the wave state based on that band width of the spectra which accounts for 50% of the wave energy. Narrow band spectra are associated with near-equilibrium single mode waves and smaller drag coefficient while broad band spectra are more associated with multi-peaked spectra, confused seas and/or non-equilibrium wave state, all leading to larger drag coefficients.

50

10.3.3 FETCH DEPENDENT MODELS

For many applications, the wave phase speed and wave age are not known. As an alternative simpler approach, the inverse wave age can be parameterized in terms of either F_*, based on the friction velocity (Perrie, Toulany 1990, Geernaert, Smith 1996), or F_u, based on the 10 m wind speed. These parameterizations are of the form:

$$u_* / C_p = w_o + \frac{\alpha}{F_*} \tag{10-14}$$

$$u_* / C_p = w_o + \frac{\alpha}{F_u} \tag{10-15}$$

where based on dimensional arguments:

$$F_* \equiv (\frac{gX}{u_*^2})^{1/3} \tag{10-16}$$

$$F_u \equiv (\frac{gX}{U^2})^{1/3} \tag{10-17}$$

Here X is the upwind fetch distance and w_o and α are determined empirically. Eq. (10-14) explains more variance than Eq. (10-15) but is characterized by self-correlation. Vickers and Mahrt (1997) find that Eq. (10-15) is a reasonable approximation for offshore flow in the coastal zone flow, although errors are larger compared to formulations based on wave state information.

Direct relationship of the roughness length to the fetch can be found in Geernaert (1988b). More complete models first describe the dependence of the wave field on fetch and then link the drag to the fetch-dependent wave field (Geernaert 1990).

10.4 Internal boundary layers

With any wind component perpendicular to the coast, internal boundary layers form due to the temperature and surface roughness contrast between the water and land surfaces. The internal boundary layer is the layer of air adjacent to the surface which is influenced by the new surface (e.g. Garratt 1990).

10.4.1 UNSTABLE CASE

With offshore flow of cold air over warmer water, a convectively driven internal boundary layer forms in response to the upward buoyancy flux over the water. This layer thickens in the downstream direction (Figure 10.2). These internal boundary layers are sometimes found to be well defined by a sharp change of properties between the convectively driven turbulence and fluid, at least in terms of instantaneous observations (Raynor et al. 1979; Sun et al. 1998b). It is not known if such sharply defined tops of the internal boundary layer are normal nor is it known if the internal boundary layer top for time-averaged flow is thick due to vacillation of the boundary-layer top.

51

Figure 10.3 shows the averaged vertical structure for a nine-hour period of stationary offshore advection of cold air observed in RASEX (Section 10.3.1). Several features occur in Figure 10.3 which are not typical of the "textbook" unstable internal boundary layer:

1) For the averaged flow, the "entrainment zone" with downward heat flux is thicker than the convective layer of upward buoyancy flux.

2) The total buoyancy-destruction of turbulence in the entrainment zone is greater than the buoyancy-generation of turbulence in the surface-based convective layer. Therefore, turbulence near the top of the internal boundary layer must be maintained by local shear-generation, as observed in Sun et al. (1998b).

3) The turbulence and stress are a maximum near the *top* of the convective layer.

4) The mean shear increases with height corresponding to convex curvature. This curvature implies inflection points near the surface and somewhere above the 45 m tower layer.
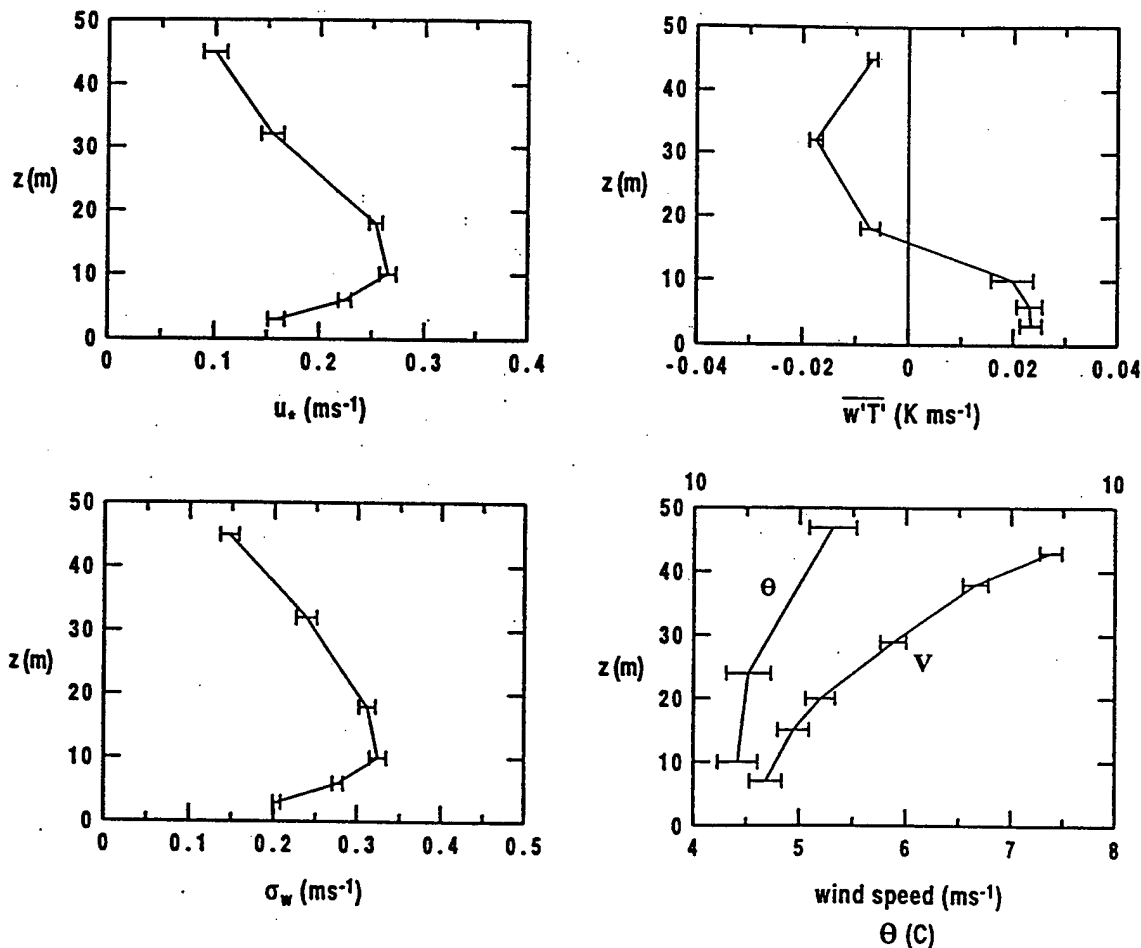
Unstable Internal Boundary Layer

Figure 10.3 The 5-hour averaged vertical structure of relative stationary offshore flow of cool air over warmer water observed in RASEX. Fluxes are based on perturbations from a 10-minute simple mean.

52

Is this structure unique to these data or does the traditional concept of internal boundary layers not apply immediately downstream from the coast? The RASEX data set is the first data set with detailed vertical resolution of the time-averaged structure in offshore flow.

Källstrand and Smedman (1997) compare various models of growth of the internal boundary layer against aircraft data collected in a developing internal boundary layer over land with onshore flow. Although most of the models have been developed for the unstable internal boundary layer over land (e.g., Melas, Kambezidis 1992; Gryning, Batchevarova 1990), they should in principal apply over the sea in the coastal zone. The internal boundary layer is traditionally modelled on two separate scales (Garratt 1990): small scales on the order of a kilometer or less and the mesoscale on a horizontal scale of tens of kilometers or more. On the scale of a kilometer or less, the heated internal boundary layer entrains upward through the old boundary layer (Vugts, Businger 1977). On this scale, the initial growth rate of the convective internal boundary layer is thought to be linearly proportional to the strength of the turbulence in the convective internal boundary layer such that (Høstrup 1981; Brutsaert 1982; Garratt 1990)

$$\frac{dh_{IBL}}{dx} = C\frac{\sigma_w}{U}$$

(10-18)

where h_{IBL} is the depth of the internal boundary layer and σ_w is the standard deviation of the turbulent fluctuations of vertical velocity, often parameterized in terms of the surface friction velocity and the convective velocity scale. The wind speed U is evaluated at the top of the internal boundary layer. Since stratification of the overlying fluid is neglected, no additional velocity scales are included. The value of C is thought to be order of unity (Mahrt 1996).

Some investigators have formulated analytical expressions for the small scale growth of the internal boundary-layer depth. For example, Andreas et al. (1979, 1981) model the depth in terms of the fetch. Observations of such internal boundary-layer growth are summarized in Andreas and Cash (1998).

Further downstream, on the mesoscale, the convective internal boundary layer completes its growth through the old boundary layer (Figure 10.2) and begins entraining nonturbulent fluid, as occurs in flow of cold air over warm water studied in Chang and Braham (1991), Smith and MacPherson (1987), Rogers et. al. (1995) and Brümmer (1996). A well-defined capping inversion usually develops and information on the stratification of the overlying fluid is required to predict further growth of the convective internal boundary layer. Models for this case are surveyed in Garratt (1990) and Källstrand and Smedman (1997).

10.4.2 STABLE CASE

The growth of the stable internal boundary layer due to flow of warm air over cooler water is expected to be slower because of buoyancy destruction of turbulence associated with the downward heat flux. For example, based on temperature profiles in Gryning (1985), the growth rate dh_{IBL}/dx in the stable internal boundary layer in the coastal zone is less than 1%. A thick residual layer of decaying turbulence extends from the top of the thin stable internal boundary layer to the top of the advected continental boundary

layer (Rogers et al. 1995). The growth of the internal boundary layer for stable conditions is also described by Mulhearn (1981) and Garratt (1990).

The vertical structure of the stable internal boundary layer may be well defined in offshore flow (e.g. Garratt, Ryan 1989) where turbulence quantities monotonically decrease with height. However, if the water temperature is much cooler than the advected air, the turbulence at the surface may collapse resulting in decoupling of the overlying advected turbulence from the surface (Figure 10.2). Such collapse cannot be predicted with existing similarity theory which is the basis for surface fluxes in numerical models. Above the surface inversion over the water, the advected turbulence from land decays in the downstream distance. Since the change of surface heat flux, viewed by a moving Lagrangian column, is almost instantaneous as it crosses the land-sea boundary, the forcing time scale due to the change of surface flux is small compared to the internal time scale of the turbulence (turbulent length scale/turbulent velocity scale). Then the turbulence decays in a self-similar fashion leading to a square root dependence on time (Sorbjan 1997).

In addition to the decaying turbulence above the surface inversion, elevated shear-generation of turbulence is observed further downstream. The flow above the surface inversion, which was part of the boundary layer over land, accelerates and forms a low level jet (Smedman et al. 1995), analogous to formation of a low-level jet above the nocturnal surface inversion (Figure 10.2). Further downstream, the shear on the underside of the jet eventually generates turbulence and re-establishes a surface-based boundary layer. Still further downstream, the flow may become near neutral as the air finally cools to the value of the sea surface temperature (Smedman et al. 1997).

The RASEX data for offshore flow of warm air over cooler water (Figure 10.4) also indicate that the classical concept of an internal boundary layer does not apply. The stress, heat and turbulence energy are smaller near the surface and reach maximum values at higher levels in the tower layer. Note that the strength of the turbulence for the stable case is comparable to that for the unstable case (Figure 10.3) because the wind speeds for the stable case are larger. For shorter periods, the stress and turbulence in the stable case may temporarily collapse near the surface in that the stress is zero within measurement error. Then the elevated turbulence is semi-detached from the surface corresponding to an upside-down boundary layer.

10.4.3 ROUGHNESS CHANGE

Internal boundary layers may also form due to spatial variation of the surface roughness between the land, shoaling zone and open ocean. With offshore flow, the smaller roughness over the sea compared to over the land leads to flow acceleration and decreased turbulence strength in the downstream direction, as observed in Smith and MacPherson (1987). Although the roughness increases in the downstream direction (Figure 10.2), it remains much smaller than the roughness over land.

Normally, at least some surface temperature discontinuity occurs at the coast so that internal boundary layers result as combination of surface roughness and surface heat flux changes. For example, Barthelmie et al. (1996) find that in unstable boundary layers associated with flow of cool nocturnal air over warmer water, winds accelerate due to smaller roughness over the water. However with stable internal boundary layers associated with daytime flow of warmer air over the water, the reduction of downward
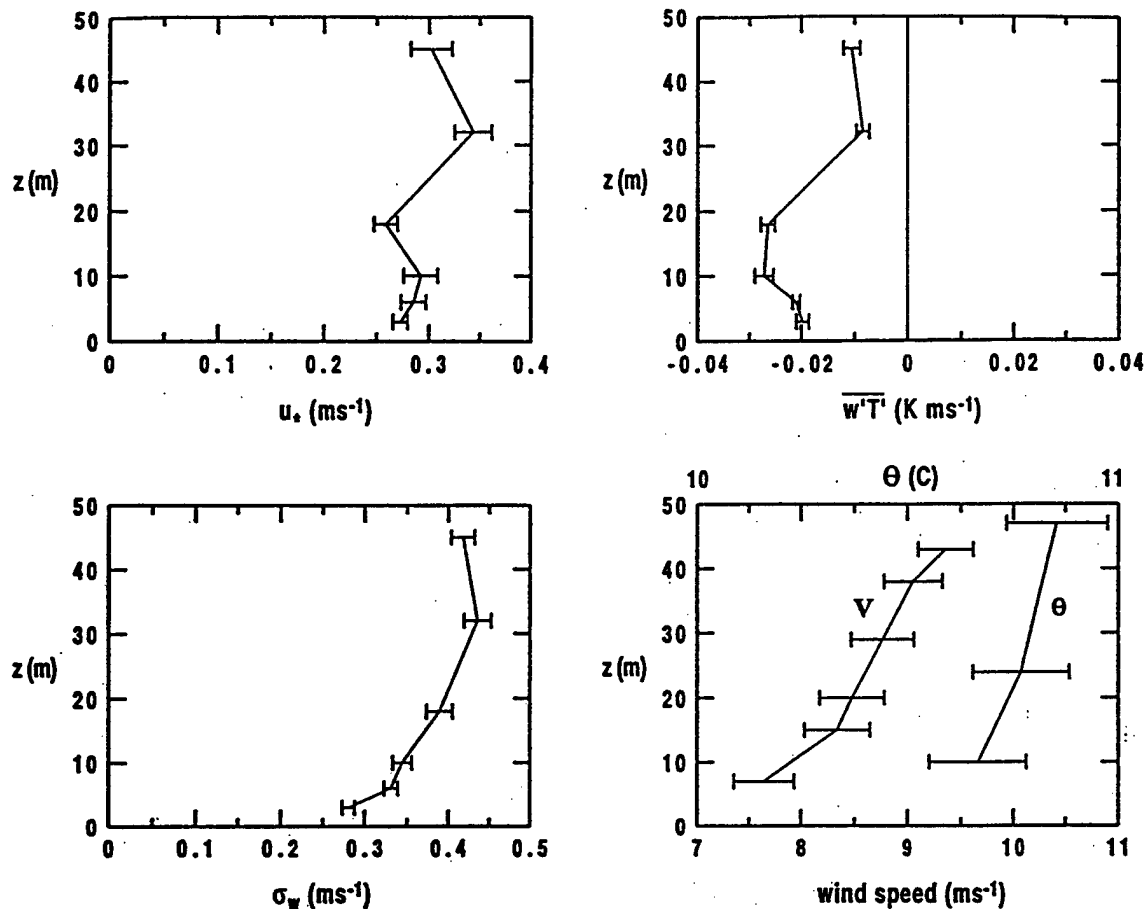
Figure 10.4 The 9-hour averaged vertical structure of relative stationary offshore flow of warm air over cooler water observed in RASEX. Fluxes are based on perturbations from a 10 minute simple mean.

mixing of momentum due to stable stratification counteracts the effect of decreased surface roughness on the wind speed. As a result, acceleration over the water was not normally observed in the daytime.

10.5 Local circulations

10.5.1 SEA/LAND BREEZES

The land-sea interface not only leads to development of internal boundary layers but also modifies the low level pressure field through differential surface heating. On sunny days, surface heat flux from the heated land surface warms the atmosphere and lowers the surface hydrostatic pressure over the land. Simultaneous heating does not occur over the water surface since: a) the heat capacity of the water is large, b) the solar radiation is absorbed over the first few meters instead of at the surface, as occurs over land, and c) heat from absorbed solar radiation is mixed downward by oceanic turbulence which is much more efficient than thermal conduction in the soil. As a result, a horizontal pressure gradient force develops directed toward the land surface. In the absence of significant opposing horizontal pressure gradient on the synoptic scale, the local

horizontal pressure gradient drives flow inland over the heated land surface, referred to as the sea breeze (Pielke 1984; Simpson 1994).

At night, surface cooling and associated downward heat flux cools the atmosphere leading to higher atmospheric pressure over the land surface. The resulting horizontal pressure gradient drives the land breeze over the sea. The nocturnal land breeze is thinner and weaker than the daytime sea breeze and is easily prevented by significant synoptic scale flow. The land breeze is rapidly eliminated by convective mixing as it flows over the warmer water (Sun et al. 1998b).

10.5.2 COASTAL TERRAIN SLOPES

Most coasts are characterized by sloping land surface. These slopes exert two independent influences on local circulations: 1) modification of the pressure field through surface heating on the sloped terrain and 2) pressure adjustments associated with topographically forced vertical motions in a stratified atmosphere. With sunny conditions, surface heating over the sloped land surface causes upslope flow in the daytime and downslope at night which augments the sea/land breeze circulation system. The slope flows may be non-hydrostatic for steep small scale slopes and approximately hydrostatic for larger scale weak slopes (Mahrt 1982).

Rising motion forced by onshore flow and sloped terrain corresponds to adiabatic cooling in the stratified atmosphere which in turn increases the underlying hydrostatic pressure. Much of this pressure increase can be associated with thickening of a cool surface marine layer capped by an inversion. The resulting local pressure gradient acts to reduce onshore flow. As a result, onshore flow decelerates before reaching the coast and the local winds at the coast are mainly parallel to the shore with rising terrain at the coast. The parallel flow may assume the form of a low level jet (Zemba, Friehe 1987).

Even flow approximately parallel to the coast experiences mesoscale disturbances induced by irregularities of the coastline. Circulations include supercritical flow (Winant et al. 1988; Samelson, Lentz 1994), coastal-trapped disturbances (Holland, Leslie 1986; Samelson, Rogerson 1996; Mass, Albright 1987), gravity currents (Dorman 1987) and a variety of other mesoscale flows (Beardsley et al. 1987). These mesoscale perturbations may be modulated by diurnal variations associated with differential surface heating, discussed above. In addition, atmospheric and oceanic circulations are coupled in the coastal zone. As one example, Zembe and Friehe (1987) examine the influence of wind acceleration and increased stress, resulting upwelling and reduction of surface temperature. The resulting increased atmospheric stability acts to reduce the stress.

10.6 Conclusions

Airflow in the coastal zone is complex due to formation of internal boundary layers, diurnally varying horizontal pressure gradients and strong spatial variation of the wave field. Assumptions required by Monin-Obukhov similarity theory may not be met due to surface heterogeneity, advection and strong vertical divergence of the flux. The surface airflow is not only coupled to the spatially varying wave field but also coupled to oceanic circulations through the sea surface temperature. Complex topography at the coast further complicate the total flow system. The above interpretive survey did not include a number of important topics such coastal zone cloud systems and special effects of bottom bathymetry. Improved understanding of fluxes in the coastal zone

must begin with observations of spatial variation of the flux with simple bathymetry, straight coast line and no significant topography.

10.7 Acknowledgments

10.8 References

Alam, A.,. Curry, J.A. (1997) Determination of surface turbulent fluxes over leads in Arctic sea ice. *J. Geophys. Res.J*, 102, 3331-3334.

Anctil, F., Donelan, M.A. (1996) Air-water momentum flux observations over shoaling waves. *J. Phy. Oc.*, 26, 1344-1353.

Andreas, E. L., Murphy, B. (1979) Velocity spectra and cospectra and integral statistics over Arctic leads. *Q. J. R. Meteorol. Soc.* 105 1053-1070.

Andreas, E. L., Williams, R. M., Paulson, C. A. (1981) Observations of condensate profiles over Arctic leads with a hot-film anemometer. *Q. J. R. Meteorol. Soc.* 107 437-460.

Andreas, E. L., Cash, B.A. (1998) Convective heat transfer over wintertime leads and polynyas. submitted to *Quart. J. Roy. Met. Soc.J*.

Beardsley, R.C., Dorman, C.E., Friehe, C.A., Rosenfeld, L.K., Winant, C.D. (1987) Local atmospheric forcing during the coastal ocean dynamics experiment. 1. A description of the marine boundary layer and atmospheric conditions over a northern California upwelling region. *J. Geophys. Res.* 92 1467-1488.

Barthelmie, R. J., Courtney, M.S., Højstrup, J., Sanderhoff, P. (1994) The Vindeby Project: A Description. Report R-741(EN), Risø National Laboratory, DK4000, Roskilde, Denmark.

Barthelmie, R. J., Grisogono, B., Pryor, S.C. (1996) Observations and simulations of diurnal cycles of near-surface wind speeds over land and sea. *J. Geophys. Res.* 101 21,327-21,337.

Beljaars, A.C. (1995) The parameterization of surface fluxes in large scale models under free convection. *Quart. J. Roy. Met. Soc.*, 121, 255-270.

Bergström, H., Smedman, A. (1995) Stably stratified flow in the marine surface layer. *Boundary-Layer Meteorol.J*, 72, 239-265.

Brutsaert, W. H. (1982) *Evaporation into the Atmosphere*. D. Reidel, Dordrecht, 299 pp.

Brümmer, B. (1996) Boundary-layer modification in wintertime cold-air outbreaks from the Arctic sea ice. *Boundary-Layer Meteorol.J*, 80, 109-125.

Chalikov, D. V., Belevich, M.Y. (1993) 'One-Dimensional Theory of the Wave Boundary Layer'. *Boundary-Layer Meteorol.J*, 63, 65-96.

Chang, S. S., Braham, R.R., Jr. (1991) Observational study of a convective internal boundary layer over Lake Michigan. *J. Atmos. Sci.J*, 48, 2265-2279.

Charnock, H. (1955) 'Wind stress over a water surface', *Quart. J. Roy. Met. Soc.J*, 81, 639-640

Davidson, K. L. (1974) Observational results on the influence of stability and wind-wave coupling on momentum transfer and turbulent fluctuations over ocean waves. *Boundary-Layer Meteorol.J*, 6, 303-323.

Deardorff, J. W. (1968) Dependence of Air-Sea Transfer Coefficients on Bulk Stability. *J. Geophys. Res.*, 73, 2549-2557.

Donelan, M. (1982) The dependence of the aerodynamic drag coefficient on wave parameters. *First International Conference on Meteorology and Air-Sea Interaction of the Coastal Zone*, Amer. Met. Soc., 381-387, 1982.

Donelan, M. (1990) Air-sea interaction, in *Ocean Engineering Science*, edited by B. Le Mehaute, and D. M. Hanes, 239-291, John Wiley and Sons.

Dorman, C.E. (1987) Possible role of gravity current in northern California's coastal summer wind reversals. *J. Geophys. Res.*, 92, 1497-1506.

Enriquez, A. G., Friehe, C.A. (1997) Bulk parameterization of momentum, heat, and moisture fluxes over a coastal upwelling area. to appear in *J. Geophys. Res.J*.

Freilich, M. H. R., Guza, R.T., Elgar, S.L. (1990) Observations of nonlinear effects in directional spectra of shoaling gravity waves, *J. Geophys. Res./*, 95, 9645-9656.

Garratt, J. R. (1990) The internal boundary layer - a review. *Boundary-Layer Meteorol./*, 50, 171-203.

Garratt, J. R., Ryan, R.F. (1989) The structure of the stably stratified internal boundary layer in offshore flow over the sea. *Boundary-Layer Meteorol./*, 47, 17-40.

Geernaert, G.L. (1988a) Influence of coastal fetch-limited waves on determining the wind stress during diabatic conditions. *Ninth Symposium on Turbulence and Diffusion*, Roskilde, Denmark, Amer. Met. Soc. 54-57.

Geernaert, G.L. (1988b) Drag coefficient modelling for the near-coastal zone. *Dyn. Atmos. Oceans*, 11, 307-322.

Geernaert, G. L.(1990) Bulk parameterizations for the wind stress and heat fluxes. *Surface Waves and Fluxes. Vol. 1 - Current Theory*, 91-172, G. L. Geernaert and W. J. Plant, Eds., Kluwer.

Geernaert, G.L., Katsaros, K.B. (1986) Incorporation of stratification effects on the oceanic roughness length in the derivation of the neutral drag coefficient, *J. Phy. Oc.*, 16, 1580-1584.

Geernaert, G. L., Larsen, S.E., Hansen, F. (1987) Measurements of the wind stress, heat flux and turbulence intensity during storm conditions over the North Sea, *J. Geophys. Res./*, 92, 13,127-13,139.

Geernaert, G. L., Davidson, K.L., Larsen, S.E., Mikkelsen, T. (1988) Wind stress measurements during the Tower Ocean Wave and Radar Dependence Experiment, *J. Geophys. Res./*, 93, 13,913-13,923.

Geernaert, G.L., Smith, J.A. (1998) `On the fetch dependent drag coefficient over coastal and inland seas', NERI Report 227, National Environmental Research Institute, Roskilde, Denmark, 10 pp.

Grachev, A. A., Fairall, C. W., Larsen, S. L. (1998) On the determination of the neutral drag coefficient in the convective boundary layer. *Boundary-Layer Meteorol./*, 86, 423-439.

Grant, A. L. M. (1992) The structure of turbulence in the near-neutral atmospheric boundary layer. *J. Atmos. Sci./*, 49, 226-239.

Garratt, J. R. (1990) The internal boundary layer - a review. *Boundary-Layer Meteorol./*, 50, 171-203.

Gryning, S.-E. (1985) The Øresund Experiment - A nordic mesoscale dispersion experiment over a land-water-land area. *Bull. Amer. Meteor. Soc./*, 66, 1403-1407.

Gryning, S.-E., Batchvarova, E. (1990) Analytical model for the growth of the coastal internal boundary layer during onshore flow. *Quart. J. Roy. Met. Soc./*, 78, 405-413.

Hansen, C., Larsen, S.E. (1997): Further work on the Kitaigorodskii roughness length model: A new derivation using Lettau's expression for steep waves. *Geophysica*, 33, 29-44.

Hare, J. E., Hara, T., Edson, J.B., Wilczak, J.M. (1997) A similarity analysis of the structure of airflow over surface waves. *J. Phy. Oc.*, 27, 1018-1037.

Högström, U. (1988) Non-dimensional wind and temperature profiles in the atmospheric surface layer: A re-evaluation. *Boundary-Layer Meteorol./*, 42, 55-78.

Højstrup, J. (1981) A simple model for the adjustment of velocity spectra in unstable conditions downstream of an abrupt change in roughness and heat flux. *Boundary-Layer Meteorol./*, 21, 341-356.

Højstrup, J. (1998) Stability effects on offshore wind profiles. submitted to *Boundary-Layer Meteorol./*.

Højstrup, J., Edson, J., Hare, J., Courtney, M.S., Sanderhoff, P. (1997) The RASEX 1994 experiments, *Risø -R-788, (ISBN-87-550-2039-9)*, 24 pp, Risø National Laboratory, Roskilde, Denmark.

Holman, R. A., Sallenger, A.H., Jr. (1985) Setup and swash on a natural beach. *J. Geophys. Res./*, 90, 945-953.

Holland, G.J., Leslie, L.M. (1986) Ducted coastal ridging over S.E. Australia. *Q. J. R. Meteorol. Soc.*, 112, 731-748.

Holland, K. T., Raubenheimer, B., Guza, R.T. (1982) Runup kinematics on a natural beach. *J. Geophys. Res./*, 100, 4985-4993.

Källstrand, B., Smedman, A-S. (1997) A case study of the near-neutral coastal internal boundary-layer growth: Aircraft measurements compared with different model estimates. *Boundary-Layer Meteorol./*, 85, 1-33.

Khanna, S., Brasseur, J.G. (1997) Analysis of Monin-Obukhov similarity from large eddy simulation. *J. Fluid Mech.*, 345, 251-286.

Kitaigorodskii, S.A. (1973) `The physics of air-sea interaction', translated from Russian, Israel Program for Scientific Translations, Jerusalem, 273 pp.

Kitaigorodskii, S.A., Volkov, Y.A., Grachev, A.A. (1995) A note on the analogy between momentum transfer across a rough solid surface and the air-sea interface. *Boundary-Layer Meteorol./*, 76, 181-197.

Kroon, L.M.M., De Bruin, H A R. (1993) Atmosphere-vegetation interaction in local advective conditions: effect of lower boundary conditions. *Agric. For. Meteorol. /*, 64, 1-28.

Large, W. G., Morzel, J., Crawford, G.B. (1995) Accounting for surface wave distortion of the marine wind profile in low-level ocean storms wind measurements. *J. Phy. Oc.*, 25, 2959-2971.

Liu, W. T., Katsaros, K.B., Businger, J.A., Tillman, J.E. (1979) Heat transport and thermal structure in the interfacial boundary layer measured in an open track of water in turbulent free convection. *J. Atmos. Sci.*, 36, 1722-1735.

Maat, N., Kraan, C., Oost, W.A. (1991) The roughness of wind waves, *Boundary-Layer Meteorol./*, 54, 89-103, 1991.

Mahrt, L. (1982) Momentum balance of gravity flows. *J. Atmos. Sci.*, 39, 2701-2711.

Mahrt, L. (1996) The bulk aerodynamic formulation over heterogeneous surfaces, *Boundary-Layer Meteorol./*, 78, 87-119.

Mahrt, L., Sun, J. (1995) The subgrid velocity scale in the bulk aerodynamic relationship for spatially averaged scalar fluxes. *Mon. Wea. Rev./*, 123, 3032-3041.

Mahrt, L., Vickers, D., Howell, J., Edson, J., Hare, J., Højstrup, J., Wilczak, J. (1996) Sea surface drag coefficients in RASEX. *J. Geo. Res., Oceans*, 101, 14,327-14,335.

Mahrt, L., Vickers, D., Edson, J., Sun, J., Højstrup, J., Hare, J., Wilczak, J. (1998) Heat flux in the coastal zone. to appear in *Boundary-Layer Meteorol./*.

Makin, V. K., Mastenbroek, C. (1996) Impact of waves on air-sea exchange of sensible heat and momentum. *Boundary-Layer Meteorol./*, 79, 279-300.

Mass, C.F., Albright, M.D. (1987) Coastal southerlies and along shore surges of the west coast of North America: Evidence of mesoscale topographically response to synoptic forcing. *Mon. Weather Rev.*, 115, 1707-1738.

Melas, D., Kambezdis, H.D. (1992) The depth of the internal boundary layer over an urban area under sea-breeze conditions. *Boundary-Layer Meteorol./*, 61, 247-264.

Miller, S., Friehe, C., Hristov, T., Edson, J. (1997) Wind and Turbulence Profiles in the Surface Layer over the Ocean. *12th Symposium on Boundary Layers and Turbulence*. Amer. Met. Soc., Vancouver, 273-274

Monin, A. S., Obukhov, A.M. (1954) Basic laws of turbulent mixing in the ground layer of the atmosphere. *Trudy Geofiz. Inst. Akad. Nauk SSSR*, 151, 163-187.

Mulhearn, P.J. (1981) On the formation of a stably stratified inertial boundary layer by advection of warm air over a cooler sea. *Boundary-Layer Meteorol./*, 21, 247-254.

Munk, W. H., Traylor, M.A. (1947) Refraction of ocean waves: A process linking underwater topography to beach erosion. *J. of Geology*, 55, 1-26. [ITEM][] Nordeng, T. E., On the wave age dependent drag coefficient and roughness length at sea, *J. Geophys. Res./*, bf 96, 7167-7174, 1991.

Oncley, S. P., Friehe, C.A., LaRue, J.C., Businger, J.A., Itsweire, E.C., Chang, S.S. (1996) Surface-layer fluxes, profiles, and turbulence measurements over uniform terrain under near-neutral conditions. *J. Atmos. Sci./*, 53, 1029-1044.

Paulson, C. A. (1970) The mathematical representation of wind speed and temperature profiles in the unstable atmospheric surface layer. *J. Appl. Meteor./*, 9, 857-861.

Perrie, W., Toulany, B. (1990) `Fetch relations for wind-generated waves as a function of wind-stress scaling', *J. Phy. Oc.*, 20, 1666-1681.

Pielke, R. A. (1984) *Mesoscale Meteorological Modeling*, Academic Press. New York, 612 pp.

Raynor, G S., Sethuraman, S., Brown, R.M. (1979) Formation and characteristics of coastal internal boundary layers during onshore flows. *Boundary-Layer Meteorol./*, 16, 487-514.

Rieder, K. F., Smith, J.A., Weller, R.A. (1994) Observed directional characteristics of the wind, wind stress and surface waves on the open ocean, *J. Geophys. Res./*, 22, 22,589-22,596.

Rieder, K.F. (1997) `Analysis of sea surface drag parameterizations in open ocean conditions', *Boundary-Layer Meteorol./*, 82, 355-377.

Rogers, D., Rogers, P., Johnson, D.W., Friehe, C.A. (1995) The stable internal boundary layer over a coastal sea. Part I: Airborne measurements of the mean and turbulent structure. *J. Atmos. Sci./*, 52, 667-683.

Samelson, R. M., Lentz S.J. (1994) The horizontal momentum balance in the marine atmospheric boundary layer during CODE-2. *J. Atmos. Sci./*, 51, 3745-3757.

Samelson, R. M., Rogerson, A.M. (1996) Life-cycle of a linear coastal-trapped disturbance. *Mon. Wea. Rev.*, 124, 1853-1863.

Simpson, J. E. (1994) *Sea Breeze and Local Winds*, Cambridge University Press, 234 pp.

Smedman, A.S., Tjernström, M., Hogström, U. (1994) `Near-neutral marine atmospheric boundary layer with no surface shearing stress: A case study', *J. Atmos. Sci./*, 23, 3399-3411.

Smedman, A-S, Bergström, H., Grisogano, B. (1997) Evolution of stable internal boundary layers over a cold sea. *J. Geophys. Res./*, 102, 1091-1099.

Smedman, A-S., Johansson, C. (1997) Modifications of Monin-Obukhov similarity theory in unstable conditions. *12th Symposium on Boundary Layers and Turbulence*. Amer. Met. Soc., Vancouver, 273-274.

Smith, S.D. (1980) Wind stress and heat flux over the ocean in gale force winds, *J. Phy. Oc.*, 10, 709-726.

Smith, S.D., Anderson, R.J., Oost, W.A., Kraan, C., Maat, N., DeCosmo, J., Katsaros,K.B., Davidson,K.L., Bumke,K., Hasse,L., Chadwick,H.M. (1992) 'Sea surface wind stress and drag coefficients: the HEXOS results', *Boundary-Layer Meteorol./*, 60, 109-142.

Smith, P.C., MacPherson, J.I. (1987) Cross-shore variations of near-surface wind velocity and atmospheric turbulence at the land-sea boundary during CASP. *Atmos-Ocean*, 25, 279-303.

Sorbjan, Z. (YEAR!!!!)Decay of convective turbulence revisited. *Boundary-Layer Meteorol./*, 82, 501-515.

Sun, J., Massman, W., Grantz, D.A., (1998a) Aerodynamic variables in the bulk formulation of turbulent fluxes. submitted to *Boundary-Layer Meteorol./*.

Sun, J., Desjardins, R., Mahrt, L., MacPherson, J.I. (1998b) Transport of carbon dioxide, water vapor and ozone by turbulence and local circulations. to appear in *J. Geophys. Res./*.

Tennekes, H. (1968) Outline of a second-order theory of turbulent pine flow. *AIAA*, 6, 1735-1740.

Thornton, E.B. (1982) Energy saturation and phase speeds measured on a natural beach. *J. Geophys. Res./*, 87, 9499-9508.

Thornton, E. B, Guza, R.T. (1983) Transformation of wave height distribution. *J. Geophys. Res./*, 88, 5925-5938.

Toba,Y., Koga, M. (1986) 'A parameter describing overall conditions of wave breaking, white capping, sea-spray production and wind stress', Oceanic Whitecaps D. Reidel, E. C. Monahan and G. Mac Niocaill Eds., 37-47.

Vickers, D., Mahrt, L. (1997) Fetch limited drag coefficients over shallow water. *Boundary-Layer Meteorol./*, 89, 53-79.

Vickers, D., Esbensen, S.K. (1998) Subgrid surface fluxes in fair weather conditions during TOGA COARE: Observational estimates and parameterization. *Mon. Wea. Rev./*, 126, 620-633.

Vickers, D., Mahrt, L. (1998) Nondimensional shear over surface waves. submitted to *Boundary-Layer Meteorol./*.

Vugts, H.F., Businger, J.A. (1977) Air modification due to a step change in surface temperature. *Boundary-Layer Meteorol./*, 11, 295-306.

WAMDI group: Hasselmann, S., Hasselmann, K., Bauer, E., Janssen, P.A.E.M., Komen, G.J, Bertotti, L., Lionello, P., Guillaume, A., Cardone, V.C., Greenwood, J.A., Reistad, M., Zambresky, L., Ewing, J.A. (1988) The WAM model - A third generation ocean wave prediction model. *J. Phy. Oc.*, 18, 1775-1810.

Wu, J. (1968) Laboratory studies of wind-wave interactions. *J. Fluid Mech.*, 68, 49-70.

Zemba, J., Friehe, C.A. (1987) The marine atmospheric boundary layer jet in the coastal ocean dynamics experiment. *J. Geophys. Res.* 92 1489-1496.

Observations of non-dimensional wind shear in the coastal zone

By DEAN VICKERS* and L. MAHRT
Oregon State University, USA

SUMMARY

Vertical profiles of the time-averaged wind stress, wind speed and buoyancy flux from the off-shore tower site in the Risø Air Sea Experiment are used to evaluate similarity theory in the coastal zone. The observed dependence of the non-dimensional wind shear on stability is compared to the traditional parametrization. Relationships between the non-dimensional shear, development of internal boundary layers and wave state are explored.

We find that the largest-scale turbulent eddies are suppressed in shallow convective internal boundary layers, leading to larger non-dimensional shear than that of the traditional prediction based only on stability. In shallow stable boundary layers, elevated generation of turbulence leads to smaller non-dimensional shear compared to the traditional prediction. Over young growing waves in stable stratification, the observed non-dimensional shear is less than that over older more mature waves in otherwise similar conditions. The non-dimensional shear is a function of wave state for stable conditions even though the observations are well above the wave boundary layer. We conclude that development of shallow internal boundary layers and young growing-wave fields, both of which are common in the coastal zone, can lead to substantial departures of the non-dimensional shear from the prediction based only on stability.

KEYWORDS: Boundary layer   Similarity theory   Turbulence

1. INTRODUCTION

Monin–Obukhov (MO) similarity theory predicts that for homogeneous and stationary conditions, the non-dimensional wind shear (ϕ_m) is a universal function of atmospheric stability alone, such that

$$\phi_m(z/L) = \frac{\kappa z}{u_*} \frac{\partial u}{\partial z} \tag{1}$$

where z is height, u is velocity, z/L is the stability parameter, L is the Obukhov length (Monin and Obukhov 1954), which is a function of the friction velocity (u_*) and the buoyancy flux, and κ is von Karman's constant. MO similarity theory applies in the surface layer above the roughness sub-layer over land, and above the wave boundary layer over water (Chalikov and Makin 1991). The top of the wave boundary layer has been defined as the height above the waves where the component of the stress in phase with the waves becomes a small fraction of the total stress. This height is thought to be approximately $\lambda/10$ (Chalikov and Belevich 1993) or $\lambda/6$ (Wetzel *et al.* 1996), where λ is the wave length of the dominant surface-wave mode. For further discussion of the wave boundary layer, see Belcher and Hunt (1998), Makin *et al.* (1995) and Large *et al.* (1995). The upper boundary of the surface layer where MO similarity theory applies is determined by the assumption that the height-dependence of the fluxes must be neglected. This normally implies that the surface layer is thin compared to the boundary layer depth. Grant (1992) has suggested that MO similarity theory should be generalized in some circumstances to include the influence of additional length scales, such as the depth of the boundary layer.

In this study, coincident measurements of vertical profiles of wind speed and vertical profiles of turbulent fluxes of momentum and buoyancy, collected during the Risø Air Sea Experiment (RASEX), are used to evaluate similarity theory hypotheses in the marine surface layer. The RASEX dataset is the first dataset with detailed vertical resolution of the time-averaged structure in off-shore flow. The RASEX off-shore flow

* Corresponding author: College of Oceanic and Atmospheric Sciences, Oregon State University, Corvallis, OR 97331, USA.

61

observations provide an opportunity to study young developing wave fields and shallow internal boundary layers (IBLs). Shallow IBLs are common in the coastal zone due to the roughness and heat flux discontinuity at the land–sea boundary (Garratt 1990; Mahrt *et al.* 1998). The observed dependence of the non-dimensional shear on z/L will be compared to the traditional land-based parametrization, and relationships between the non-dimensional shear, wave state and IBL development will be explored.

2. SIMILARITY THEORY

The non-dimensional shear of MO similarity theory has typically been evaluated by measuring the turbulent fluxes at a height thought to be in the surface layer, often taken as 10 m, and the shear from the mean wind speed at 2 levels which encompass the turbulence measurements. Data collected over land in several field programmes (e.g. Businger *et al.* 1971; Dyer 1974; Högström 1988) have been used to fit empirically the functional form of $\phi_m(z/L)$. These studies have generally confirmed that the non-dimensional shear appears to be a universal function of z/L. A commonly used parametrization (Dyer 1974) based on data from these field programmes is

$$\phi_m(z/L) = \{1 - 16(z/L)\}^{-1/4}; \quad z/L < 0 \tag{2}$$

$$\phi_m(z/L) = 1 + 5(z/L); \quad z/L > 0. \tag{3}$$

An alternative formulation for the stable case, proposed by Beljaars and Holtslag (1991), is

$$\phi_m(z/L) = 1 + \frac{z}{L}\left\{a + b\,e^{-d\frac{z}{L}}\left(1 + c - d\frac{z}{L}\right)\right\} \tag{4}$$

where $a = 1, b = 0.667, c = 5$, and $d = 0.35$.

In local similarity theory, the turbulent fluxes and stability are not constrained to be constant with height and the non-dimensional shear takes the form (e.g. Wyngaard 1973; Nieuwstadt 1984; Sorbjan 1986)

$$\phi_{ml}(z/\Lambda) = \frac{\kappa z}{u_{*l}}\frac{\partial u}{\partial z} \tag{5}$$

where the subscript l refers to the local value at a given height, and Λ is the value of L calculated from the local height-dependent fluxes. This theory recognizes that local fluxes should be related to the local shear and stability. When the height-dependence of the fluxes of momentum and buoyancy can be neglected, local similarity reduces to MO similarity. In this sense, MO similarity is a subset of local similarity. Studies that report ϕ_m based on measuring fluxes at a single level, e.g. the 10 m level on a tower, are formally evaluating local similarity theory (ϕ_{ml}) due to a lack of information on the change in the fluxes with height. The distinction between MO and local similarity theory becomes uncertain in studies that do not evaluate the height-dependence of the flux. Previous single-level studies have been postulated as MO similarity by implicitly assuming that the height-dependence of the flux can be neglected. This is probably a good assumption in the lowest few tens of metres in the daytime convective boundary layer. However, with internal boundary layers or morning and evening boundary layer transition periods, which are the main source of near-neutral data in many field programmes, this assumption breaks down. Therefore, some observational studies have computed stability functions intended for MO similarity when in actuality the stability functions are more appropriate to local similarity theory.

According to traditional similarity theory, the non-dimensional shear does not depend on any characteristics of the surface. Historically, the surface has been represented by the roughness length (z_o), which is the constant of integration obtained when integrating Eq. (1) with respect to z to obtain $\psi_m(z/L)$ (e.g. Paulson 1970). Over solid surfaces, the roughness length is usually considered to be a constant for a given location, and dependent on wind direction over heterogeneous surfaces. The roughness length for momentum is found to be directly related to the physical size and spacing of the roughness elements of the surface.

Unlike conditions over land, the sea surface roughness field consists of a broad band of waves which are generated by and interact with the mean wind. With accelerating winds, surface gravity waves grow by extracting momentum from the mean flow, while with decelerating winds and mature waves, the surface wave field extracts considerably less energy or even loses energy to the mean flow. The wind and waves in the coastal zone are often in non-equilibrium due to bathometry and limited fetch. Sea surface roughness lengths are much smaller than typical land values. Over the sea, the roughness length has been parametrized using the Charnock (1955) relationship, which predicts that the roughness length is proportional to the wind stress.

Numerous studies have found that for a given wind speed and stability parameter (z/L), the drag coefficient and roughness length are larger over young and developing wave fields compared with older wave fields that are more in quasi-equilibrium with the wind (e.g. Kitaigorodskii 1970; Snyder et al. 1981; Geernaert et al. 1987; Donelan, 1990; Smith et al. 1992; Donelan et al. 1993; Vickers and Mahrt 1997a). Wave age is often used as a measure of the maturity of the wave field, and is typically calculated as the ratio of the wave phase speed of the dominant wave mode (C_p) (assuming a dominant mode is well defined) to either the friction velocity or the wind speed at some level near the surface (e.g. 10 m). The effect of wave age has been parametrized within the existing framework of similarity theory by formulating the roughness length, or equivalently the neutral drag coefficient, as a function of wave age (e.g. Toba and Koga 1986; Maat et al. 1991; Donelan 1990; Smith et al. 1992).

Some studies have approached the influence of wave state by directly examining the dependence of ϕ_m (or equivalently ψ_m and a specified z_o) on wave state rather than adjusting the roughness length. Bergström and Smedman (1995) found that the non-dimensional shear was less with young waves (small wave-age parameter) compared to old waves, but concluded that the relationship was not statistically significant, perhaps due to their small range of conditions. However, their result is consistent with enhanced mixing and stress over young, growing waves. Davidson (1974) found that isolating the dependence of the non-dimensional shear on wave state is sensitive to how the stability dependence is removed. He concluded that for his open-ocean dataset, the non-dimensional shear increased with wave age, in contrast to traditional MO similarity theory which contains no wave state dependence. In his dataset, the wave field was characterized as surge swell (values of $C_p/u_* > 25$) representative of an older decaying wave field, conditions were always stable $(z/L > 0)$, and almost all results were based on a single vertical level (8 m). Consistent with enhanced mixing over younger waves, Davidson (1974) suggested a form $\psi_m(z/L, C_p/u_*)$, where ψ_m decreased with wave age for $C_p/u_* > 25$.

Miller et al. (1997) reported observational evidence in near-neutral conditions for an intermediate layer of order 10 m thickness located above the wave boundary layer (order 1 m) and below an outer logarithmic layer. In the intermediate layer, the wind shear was substantially less than predicted by MO similarity (smaller ϕ_m than predicted). They found that the wave-induced stress associated with atmospheric motions in phase with

63

the surface waves was significant in the underlying wave boundary layer and was small in the intermediate layer.

In the coastal waters of the Baltic Sea, Smedman et al. (1995) found that in stable flow, the non-dimensional wind shear and temperature gradient based on observations 8 m above the sea surface did not always agree with traditional MO similarity. They attributed this to an extremely shallow surface layer due to the presence of a low-level jet (30 to 150 m) and suggested that the height of the jet may be an important length scale. Smedman et al. (1995) proposed that the low-level jet suppresses low-frequency motions thus reducing the transport and increasing the non-dimensional wind shear. They found general agreement with traditional MO similarity at the same site during similar stability when no low-level jet was detected.

Grant (1992) suggests that the non-dimensional gradient $\phi(z/L)$ for the near-neutral boundary layer should be generalized to be of the form $\phi(z/h, h/L, u_*/fh)$ in order to include the influence of boundary layer depth (h) on the non-dimensional shear. Khanna and Brasseur (1997) consider the form $\phi(z/L, h/L)$ where their ϕ is the non-dimensional gradient of an arbitrary variable. In the large eddy simulation results of Khanna and Brasseur (1997), the non-dimensional shear decreases above the surface layer; this is also observed by Smedman and Johansson (1997) in shallow off-shore boundary layers. Apparently, the vertical gradient decreases more rapidly with height above the surface than does the flux. No specific formulation for a generalization of ϕ to include the dependence on boundary layer depth has been attempted. If the influence of boundary layer depth on ϕ_m extends downward to the surface, or if the influence of wave state on ϕ_m extends upward above the wave boundary layer, then both local and MO similarity theory break down. We intend to consider several possibilities: (a) MO similarity with existing stability functions is valid; (b) MO similarity theory is valid but the traditional stability functions require modification; (c) MO similarity is not valid but local similarity is appropriate with possible modification of the stability functions; and (d) both local and MO similarity theory are invalid and additional information such as boundary layer depth and wave state are required.

3. DATASET

The full RASEX instrumentation is described in Barthelmie et al. (1994) and Højstrup et al. (1997). Data used in this study were collected at the sea mast west tower located 2 km off the coast of Lolland, Denmark in 4 m of water. Observations taken from April through November 1994, including the intensive campaigns during the spring and autumn, are considered. The off-shore tower site is representative of an inland sea or large lake, with only small amplitude swell and predominantly wind driven waves with characteristic amplitudes less than 1 m and wavelengths less than 16 m (Vickers and Mahrt 1997a). In strong on-shore flow, the wave boundary layer may sometimes include the lowest turbulent flux measurement level at 3 m (Hare et al. 1997). The lowest observational level used in this study (6 m) is expected always to be above the top of the wave boundary layer based on the maximum observed wavelength. Shallow IBLs are common in off-shore flow where the fetch ranges from 2 to 5 km (Mahrt et al. 1998). On-shore flow, where the fetch ranges from 15 to 25 km, is still fetch-limited compared to the open ocean.

Fast-response (20 Hz) observations from Gill/Solent sonic anemometers (hereafter sonics) positioned 6, 10, 18 and 32 m above the sea surface were used to estimate the turbulent wind stress and buoyancy flux profiles. Turbulence measurements from

the instrument at the 3 m level were excluded in this study due to potential flow-distortion problems. Fluxes calculated from the 45 m level sonic data were found to be erratic and unreliable, presumably due to an instrumental problem, and were excluded. The tilt-correction method used for the sonics was presented in Mahrt et al. (1996). The buoyancy flux was calculated from the sonic virtual-temperature fluctuations, after applying a correction for acoustic wave bending that can be important in strong winds. Vertical profiles of wind speed were measured using cup anemometers (P224b sensor) located 7, 15, 20, 29 and 38 m above the sea surface. Time periods where the cup anemometer wind speed was less than 2.5 m s^{-1} were excluded; because the cup anemometers were calibrated for the generally strong winds at the site, readings of less than 2.5 m s^{-1} are not reliable. Temperature profiles were measured using a thermometer at 10 m (Risø PT 100), and temperature-difference sensors (Risø PT 500) to provide the vertical gradient of temperature over the layers 10 to 24 m and 10 to 47 m. The fluctuating wave height was measured using an acoustic wave recorder. A characteristic wave amplitude, wave phase speed and wavelength were calculated as described in Vickers and Mahrt (1997a). All time periods with wind direction from the sector including 339 deg. through 106 deg. were excluded, because of potential tower interference and possible flow distortion due to wind turbines located north-east of the tower.

The sonic and cup anemometer and wave recorder measurements were subjected to quality control screening as described in Vickers and Mahrt (1997b). The automated quality control procedure identifies periods with potential problems with instruments or data recording. The package of tests checks for excessive electronic spiking, inadequate amplitude resolution, signal dropout, unrealistic magnitude, extreme higher moment statistics and near discontinuities in the first two moments. Visual inspection of all data flagged by the automated procedures was carried out, either to verify an instrument problem or to identify unusual but plausible atmospheric behaviour. In the former case, the flag was verified and the data were eliminated.

Direct observations of IBL depth at the site were not routinely available during RA-SEX. Profiles of potential temperature, humidity and winds, measured by tethersondes released from land in the vicinity of the site during 12 different days in October and early November 1994, were examined. A parametrized IBL depth (e.g. Højstrup, 1981)

$$h = C\sigma_w(X/u), \qquad (6)$$

where σ_w is the vertical velocity fluctuation, X is the fetch distance and C is an empirical coefficient, was found to correlate reasonably well with the IBL depth as inferred from the tethered balloon soundings for the limited number of comparisons available. We found that setting $C = 0.4$ gave a better fit to the data than the original coefficient of unity, and use $C = 0.4$ in all further calculations. Using the vertical velocity fluctuations from the 18 m sonic, the 38 m wind speed from the cup anemometer and the actual fetch distance, the parametrized h at the tower location varies from a minimum of 20 m in off-shore flow (1:100 stable IBL growth rate) to a maximum of 400 m in on-shore flow (1:30 unstable IBL growth rate). We note that u in Eq. (6) should represent the mean wind at the top of the IBL, which results in an iterative expression for h. Here, we approximate u at height h using the 38 m wind speed.

(a) Fluxes

Eddy correlation fluxes of momentum and virtual temperature were calculated from sonic anemometers at 4 levels (6, 10, 18 and 32 m) to estimate profiles of the wind

stress and Obukhov length. An averaging time-scale of 10 minutes was selected to define the turbulent fluctuations, and the flux computed from such fluctuations was averaged over one-hour periods. Therefore, the fluxes include all motions on time-scales of 10 minutes or less down to the smallest resolvable scales determined by the sampling rate (20 Hz). These averaging times were chosen to optimize the correlation between the mean wind speed and the wind stress (Mahrt *et al.* 1996). Averaging times longer than one hour incorporate too much non-stationarity, and shorter averaging times do not include enough samples. Elimination of records with large non-stationarity and flux sampling errors are discussed in the appendix. The wind stress was calculated as the vector magnitude of the one-hour averages of the stress components.

(b) Wind profiles

The wind shear was estimated by applying the method of least squares to fit a second-order polynomial in $\ln(z)$ to the profiles of one-hour mean wind speed from the cup anemometers at 5 levels (7, 15, 20, 29 and 38 m), and also a derived level at the roughness height (z_o) where the wind speed was assumed to be zero. The precise heights of the wind speed measurements were adjusted to account for the fluctuating mean sea level. The wind speeds from the cup anemometers were re-calibrated using the post-experiment calibration coefficients (Højstrup, personal communication). The wind shear was evaluated analytically at the flux measurement heights (6, 10, 18 and 32 m) using the coefficients of the second-order polynomial fit to the wind speed profile as in Högström (1988). The Charnock relationship with a coefficient of 0.017 (Garratt 1977) was used as a lower-boundary condition for the fit. The fit to the wind speed profile was not sensitive to the choice of this coefficient nor application of a wave-age dependent Charnock relationship.

As a sensitivity study, the wind speed profiles were fitted using the cup anemometer wind speeds alone, the sonic speeds alone and a combined set of cup and sonic wind speeds. We also calculated the shear using finite differences applied to adjacent cup levels, differencing with respect to both linear z and $\ln(z)$. In most instances, the profile of wind speed from the cups was smoother than both the profile from the sonics and the profile from the combined cup and sonic set. In terms of variance explained, the cup wind speed profiles were better represented by the second-order polynomial than were the profiles from the sonic speed measurements or the combined cup and sonic set. The root-mean-square error of the model fit to the wind speed profile evaluated at the 5 cup anemometer levels ranged from 0.03 m s^{-1} to 0.19 m s^{-1} and averaged 0.09 m s^{-1}.

4. NON-DIMENSIONAL SHEAR

The observed dependence of ϕ_{ml} on z/Λ for all the data including all 4 vertical levels and both on-shore and off-shore flow regimes is shown in Fig. 1. The observed ϕ_{ml} is less than the traditional prediction (Eqs. (2)–(4)) for the entire range of stability (greater stress relative to the shear). The near-neutral $(-0.01 < z/\Lambda < 0.01)$ value of ϕ_{ml} is 0.95 with $\kappa = 0.40$. The standard error of the average ϕ_{ml} for z/Λ categories is relatively small for the near-neutral categories, and larger for unstable and stable categories where the number of observations is less.

For estimating ϕ_m for MO similarity at the 10 m level, we excluded cases with the largest vertical flux divergence based on the fluxes at the 6, 10 and 18 m levels. This flux divergence criterion excluded approximately one-half of the data. For the remaining cases used in calculating ϕ_m, the magnitude of the stress divergence for the layer from
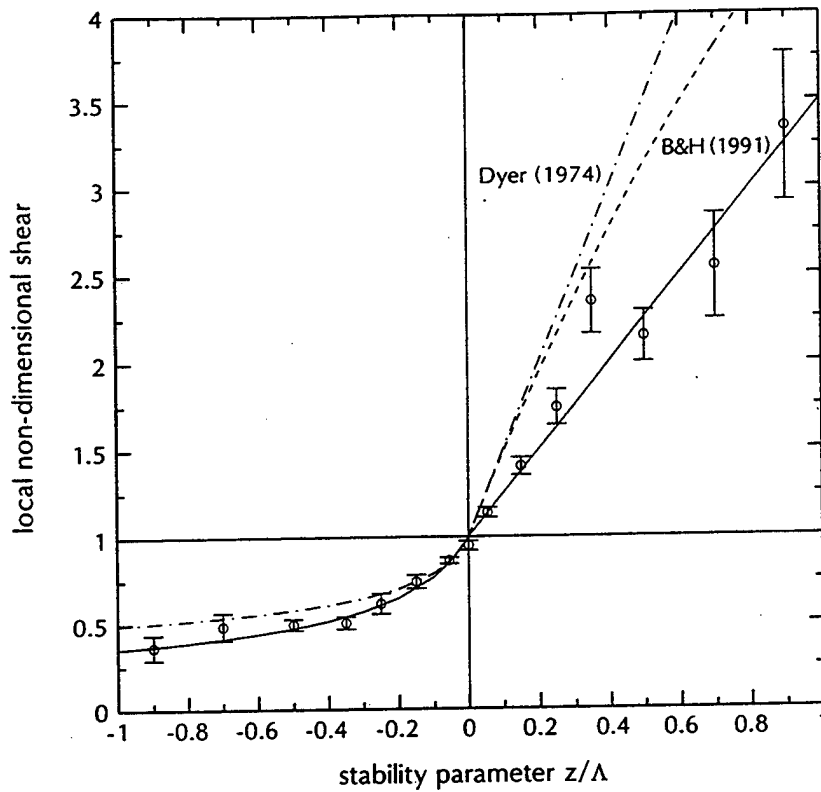
Figure 1. The mean (circles) and plus and minus one standard error of the local non-dimensional shear (ϕ_{ml}) for stability (z/Λ) categories (see text) for all the data. The solid curve is a fit to the data: $\phi_{ml} = \{1 - 7(z/\Lambda)\}^{-1/2}$; $z/\Lambda < 0$, and $\phi_{ml} = 1 + 2.5(z/\Lambda)$; $z/\Lambda > 0$, where Λ is the Obukhov length based on local fluxes. The dash-dot curve is the traditional Dyer (1974) parametrization. The dashed curve is the Beljaars and Holtslag (1991) formula.

6 m to 18 m was always less than 8×10^{-3} m s^{-2} and averaged 5×10^{-4} m s^{-2}. As we found for local similarity, the non-dimensional shear of MO similarity theory (ϕ_m) is also less than the traditional prediction (Fig. 2). The mean ϕ_m at 10 m for weakly stable conditions is larger than ϕ_{ml}, closer to both the predictions (Eqs. (3)–(4)) and similar to the estimate of ϕ_{ml} when excluding off-shore flow cases (Fig. 3). This reflects the fact that large flux divergence is common in off-shore stable flow. In this regard, eliminating periods with large flux divergence is similar to eliminating periods with stable off-shore flow. In unstable conditions, the observed 10 m ϕ_m is less than ϕ_{ml}, further from the prediction (Eq. (2)) and similar to ϕ_{ml} when excluding shallow IBL cases (Fig. 4). For the unstable case, eliminating periods with large flux divergence also tends to eliminate periods with shallow IBL depth. We conclude that eliminating convective cases with large flux divergence does not improve the agreement between the observed ϕ_m and the traditional prediction (Eq. (2)).

Note that the range of the stability parameter for the ϕ_m dataset, where $z = 10$ m, is considerably less than for the ϕ_{ml} dataset which includes $z = 6$, 10, 18 and 32 m. The standard error bars are larger for ϕ_m than for ϕ_{ml} partly due to the smaller sample size.

The mean $\phi_{ml}(z/\Lambda)$ partitioned into on-shore and off-shore flow categories is shown in Fig. 3. In this dataset, the majority of the strongly convective cases are found in on-shore flow while the majority of the strongly stable cases are found in off-shore flow. This complicates attempts to isolate the effects of stability and fetch. The range of z/Λ for an individual stability category was expanded in Fig. 3 compared to Fig. 1,
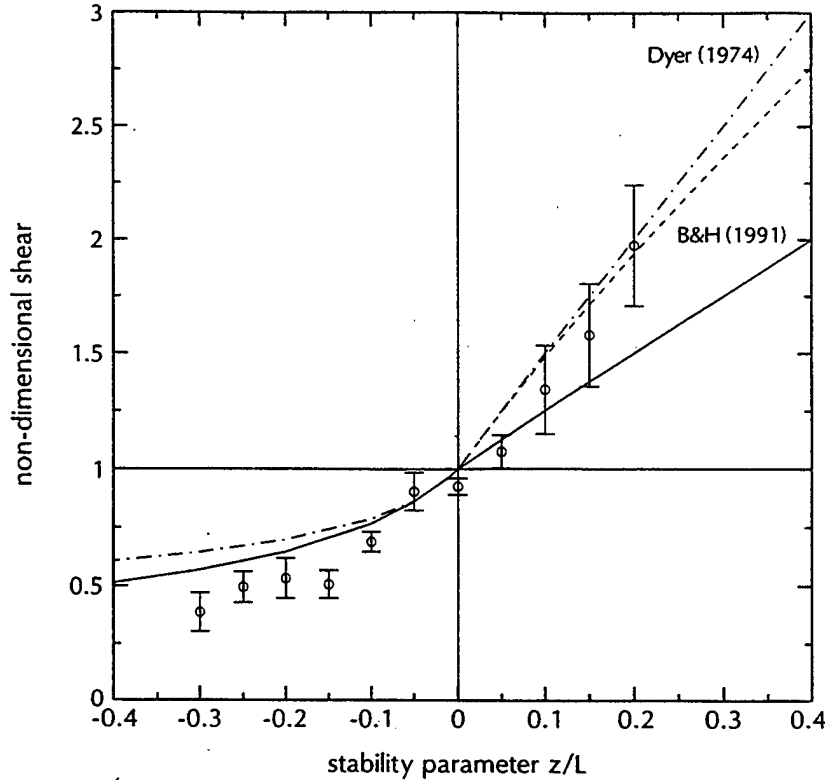
Figure 2. The mean and standard error of the non-dimensional shear (ϕ_m) for 10 m data only for stability (z/L) categories (see text). The solid curve is a fit to the local non-dimensional shear ϕ_{ml} (as in Fig. 1). The dash-dot curve is the traditional Dyer (1974) parametrization. The dashed curve is the Beljaars and Holtslag (1991) formula.

to ensure an adequate number of samples in each stability category when partitioning the data by both stability and flow regime. For off-shore neutral and stable flow, ϕ_{ml} is significantly less than predicted by previous relationships. In the transition region downstream from a rough-to-smooth roughness change, the mean shear may adjust more rapidly to the smoother ocean surface compared to the stress, preventing equilibrium between the stress and the shear (Peterson 1969). As a result, the non-dimensional shear may be smaller in the coastal zone than that predicted by traditional similarity theory. A mechanism to account for the difference between the on-shore and off-shore flow unstable cases is discussed next.

(a) IBL depth

The stability dependence of ϕ_{ml} for two z/h categories is shown in Fig. 4 where h is the IBL depth estimated from Eq. (6). The largest values of z/h (small h) occur in off-shore flow due to the shorter fetch, and partitioning the data by z/h also tends to partition the data into off-shore and on-shore flow regimes. Therefore, other factors in addition to IBL depth may cause differences between the two z/h classes.

In convective IBLs, ϕ_{ml} increases with increasing z/h with the exception of the most unstable category, that also has the least amount of data. We attribute the increase of ϕ_{ml} with increasing z/h to suppression of the largest convective eddies by the shallow IBL top (Mahrt et al. 1998), which acts to reduce the stress relative to the shear. Multi-resolution spectra (Howell and Mahrt 1997) of the wind stress from the 6 and 32 m levels support this theory in that lower-frequency (large eddy) transport is indeed suppressed
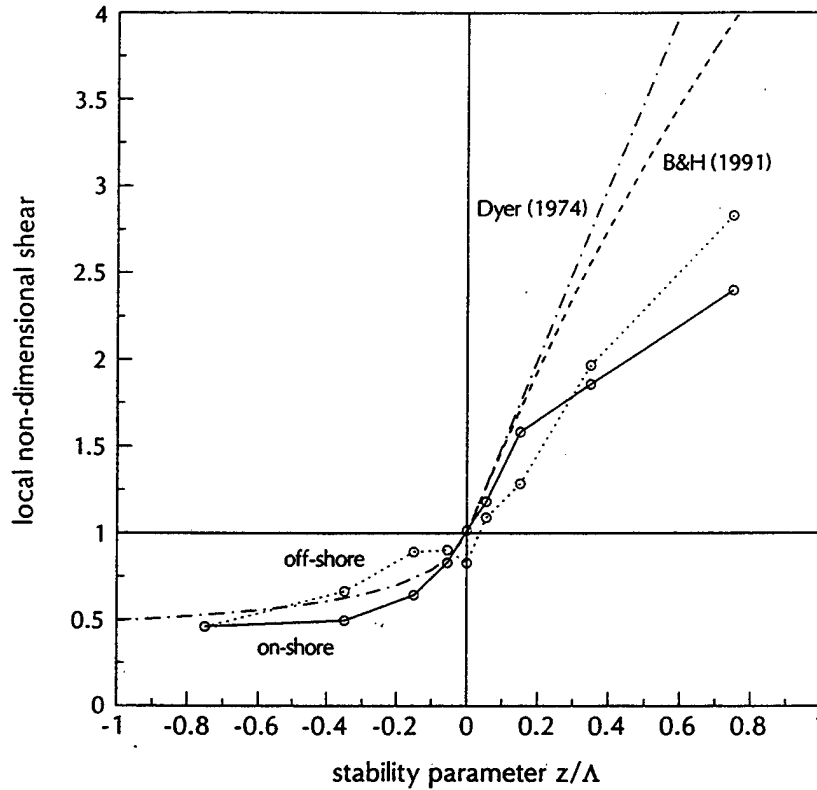
Figure 3. The mean local non-dimensional shear (ϕ_{ml}) for stability (z/Λ) categories (see text) for on-shore flow (solid) and off-shore flow (dotted). The dash-dot curve is the traditional Dyer (1974) parametrization. The dashed curve is the Beljaars and Holtslag (1991) formula.

by shallow IBL depth (Fig. 5). The multi-resolution spectra orthogonally decompose the flow into simple unweighted averages for different averaging windows. These spectra yield results similar to Fourier spectra but satisfy Reynolds averaging at all scales and do not assume periodicity.

In contrast to unstable conditions, the spectra for neutral and stable conditions show little difference in the scale-dependence of the stress over a wide range of z/h. Our hypothesis is that in neutral and stable conditions, the eddies are too small to be suppressed by the shallow IBL depth.

The agreement with traditional similarity for convective IBL cases is better when combining on-shore and off-shore flow (Fig. 1), than when partitioning the data by either flow regime or z/h (Figs. 3 and 4). This agreement is somewhat circumstantial. In on-shore flow, where the IBL depth is typically large compared to the observation height, and where we would expect the best agreement with the traditional parametrization, ϕ_{ml} is less than predicted. In off-shore flow with shallow convective IBLs, ϕ_{ml} is larger than predicted. *These data suggest that for the convective case, ϕ_{ml} is less than predicted by traditional similarity but increases with increasing z/h.*

In stably stratified IBLs, ϕ_{ml} decreases with increasing z/h (Fig. 4). That is, shallow stable IBLs lead to relatively large stress and therefore smaller ϕ_{ml} than predicted. We attribute this to the top-down nature of the turbulence in the presence of shallow stable IBLs in advective conditions where the stress decreases with height more slowly than the mean shear, or where it may even increase with height (Fig. 6). This is apparently due to suppression of turbulence near the surface by the stratification in concert with
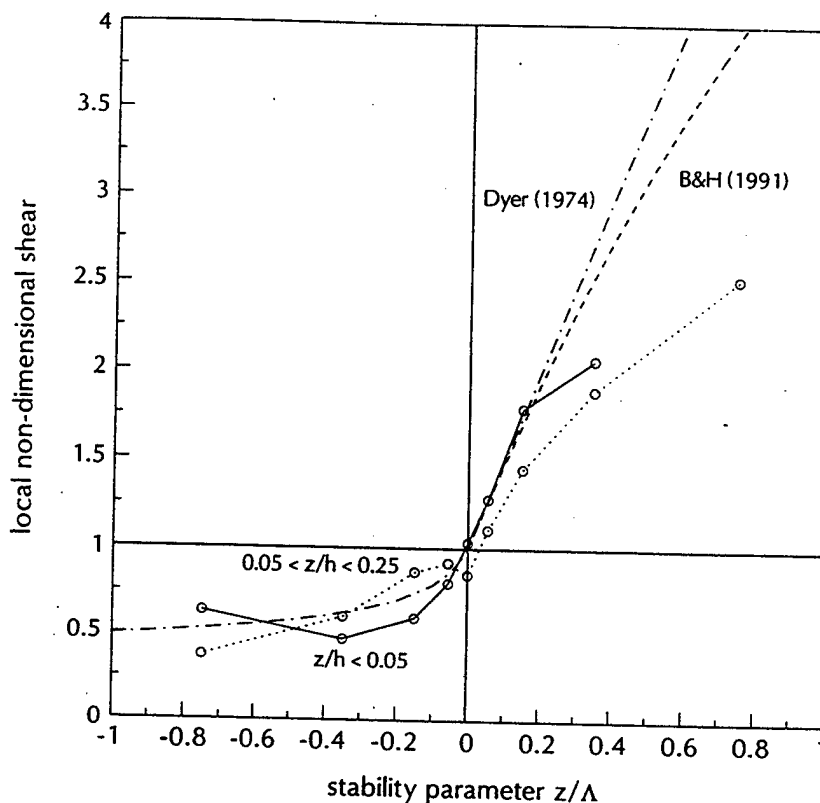
Figure 4. The mean local non-dimensional shear (ϕ_{ml}) for stability (z/Λ) categories (see text) for two internal boundary layer (IBL) depth (z/h) categories: (i) $z/h < 0.05$ (solid); and (ii) $0.05 < z/h < 0.25$ (dotted), where h is the parametrized IBL. The dash-dot curve is the traditional Dyer (1974) parametrization. The dashed curve is the Beljaars and Holtslag (1991) formula.

shear-generation of turbulence aloft, although horizontal advection of turbulence may also be important. The composited wind profiles for this case (not shown) correspond to increasing mean shear with height. The elevated shear may be associated with flow acceleration resulting from partial decoupling from the sea surface, sometimes observed with the flow of warmer air over cooler water (Smedman *et al.* 1995). When the stress increases with height the usual atmospheric boundary layer is turned upside down, in that the primary source of the turbulence is aloft rather than at the surface. The physical interpretation of the IBL depth is ambiguous in such cases.

Temperature advection is also important in off-shore flow. Non-zero heat flux is forced primarily by temperature advection. That is, the heat flux divergence is balanced by temperature advection since the local time-change of temperature is usually small. Since z/L depends on the heat flux, z/L is correlated with temperature advection. Therefore, any stability-dependent non-dimensional quantities over the sea automatically contain advective effects, particularly in the coastal zone.

(b) Wave age

The stability dependence of ϕ_{ml} for two wave age (C_p/u_*) regimes is shown in Fig. 7. Young, growing-wave fields preferentially occur with off-shore flow, but are also commonly found in strong on-shore flow. In stable conditions, ϕ_{ml} increases significantly with increasing wave age as also observed by Bergström and Smedman (1995) and Davidson (1974). The self-correlation between wave age and ϕ_{ml} (both
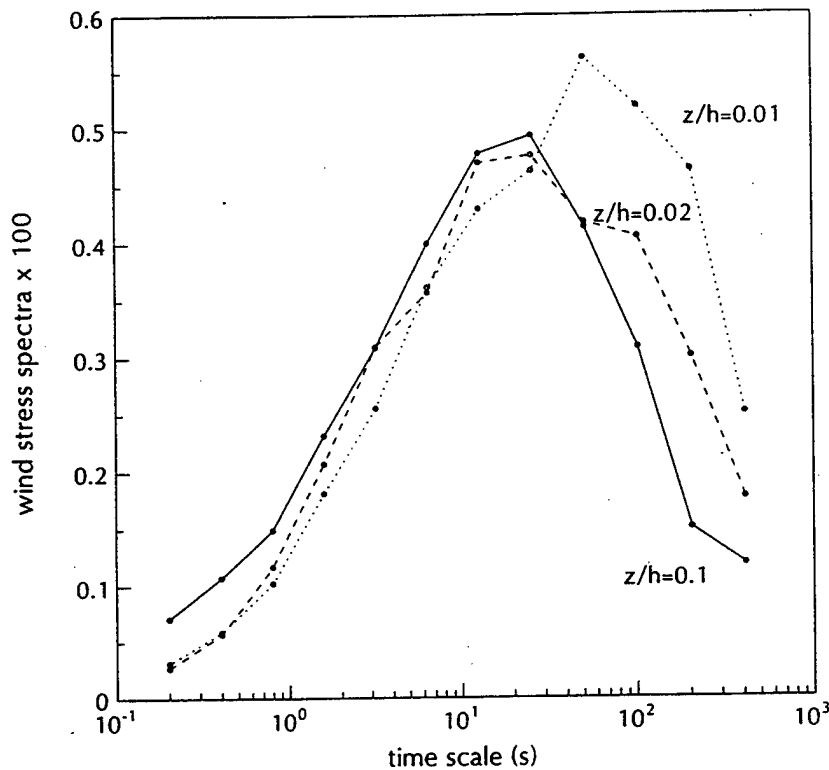
Figure 5. Average multi-resolution spectra of the one-hour average kinematic wind stress ($m^2 \, s^2 \times 100$) at the 6 m level in unstable conditions for three z/h categories (see text): (i) $z/h = 0.1$ (solid); (ii) $z/h = 0.02$ (dashed); and (iii) $z/h = 0.01$ (dotted) where h is the parametrized internal boundary layer depth. The time-scale axis is analogous to the period in Fourier analysis.

contain u_*) may influence the result. The self-correlation between z/L and ϕ_m can also be large (L contains u_*^3). We have attempted to reduce the self-correlation by jointly stratifying ϕ_{ml} by both z/Λ and C_p/u_* in Fig. 7. In a separate calculation, we partitioned the data into C_p/u_t wave-age regimes, where this wave-age parameter is based on u_t, the estimated wind speed at the top of the wave boundary layer, instead of u_*, and thus is not subject to self-correlation. This calculation confirmed a real dependence of ϕ_{ml} on wave state. We conclude *that in stable conditions, the mean shear does not completely adjust to the growing-wave field leading to a dependence of ϕ_{ml} on wave age.*

The possible dependence of ϕ_{ml} on wave age contradicts the assumption of similarity theory that the local flux-gradient relationship in the surface layer is independent of surface conditions. In traditional similarity theory for the surface layer (above the wave boundary layer), the influence of surface characteristics is included in the roughness length which appears in the vertical integration of ϕ_{ml} downward to the surface. In this dataset, the observation heights are well above the estimated wave boundary layer height, so that dependence of ϕ_{ml} on wave state is not expected on the basis of traditional similarity theory.

For unstable conditions, ϕ_{ml} is observed to be larger over younger waves, contrary to the result found for stable flow (Fig. 7). This may be due to the dominant influence of shallow IBL depth rather than wave state in modifying ϕ_{ml} for convective cases (section 4(a)). It may also be related to correlation between wave age and other processes related to flow direction, since the difference between ϕ_{ml} for younger waves compared
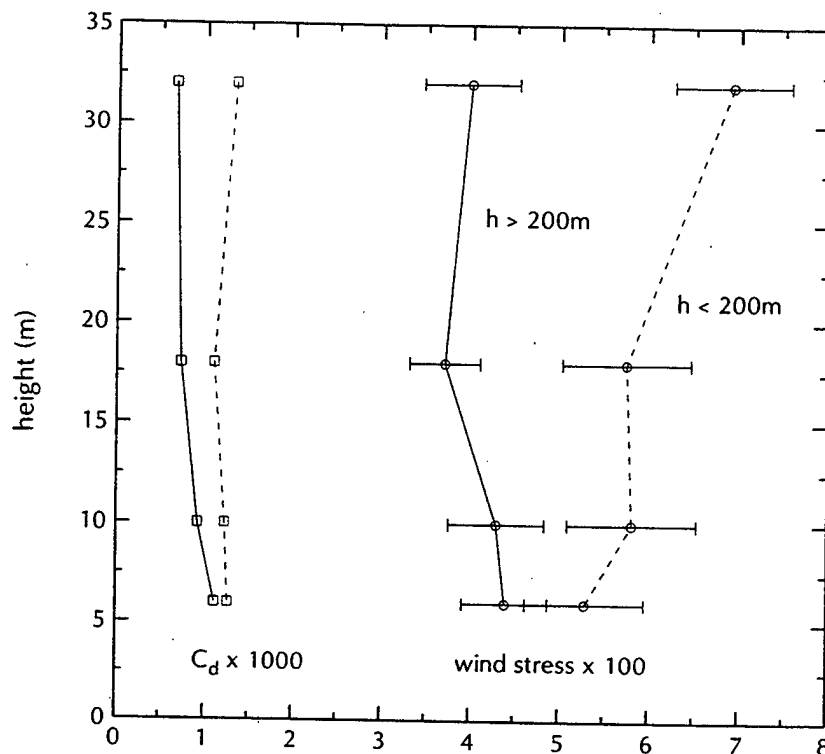
71

Figure 6. Average profiles of the kinematic wind stress ($m^2s^2 \times 100$) and drag coefficient ($C_d \times 1000$) in stable stratification ($0.05 < z/L < 0.3$) for $h > 200$ m (solid) and $h < 200$ m (dashed) where h is the parametrized internal boundary layer depth, and Obukhov length L is calculated using the average fluxes from the 6 and 10 m levels. The average stability (z/L) and wind speed profile for both h categories are nearly identical.

with older waves is similar to the difference when partitioning the data by flow direction (Fig. 3).

5. NEW FORMULATION

With off-shore flow in the coastal zone, shallow IBL's are common due to short fetch. Significant vertical stress and buoyancy flux divergences are typical due to shallow IBL depth and strong temperature advection. The wind and waves can be in non-equilibrium due to the bathometry and limited fetch. Relatively large stress generated over land may be advected over the water. The mean flow normally accelerates due to smaller surface roughness over the water. All of these mechanisms influence the non-dimensional shear.

We expect that the conditions required for application of similarity theory will be best satisfied when advective effects are minimal (on-shore flow) and the observation height is sufficiently below the IBL depth ($z/h < 1/4$). The stability dependence for data satisfying these conditions is shown in Fig. 8 and a fit to the data is:

$$\phi_{ml} = \{1 - 35(z/\Lambda)\}^{-1/4}; \ z/\Lambda < 0 \tag{7}$$

$$\phi_{ml} = \{1 + 16(z/\Lambda)\}^{1/3}; \ z/\Lambda > 0. \tag{8}$$

For this reduced dataset, a von Karman constant (κ) equal to 0.39 is required to make $\phi_{ml}(z/\Lambda = 0)$ equal to unity, and the coefficients in Eqs. (7)–(8) are based on $\kappa = 0.39$. The model predicts unstable values of ϕ_{ml} that are approximately 15–20% smaller
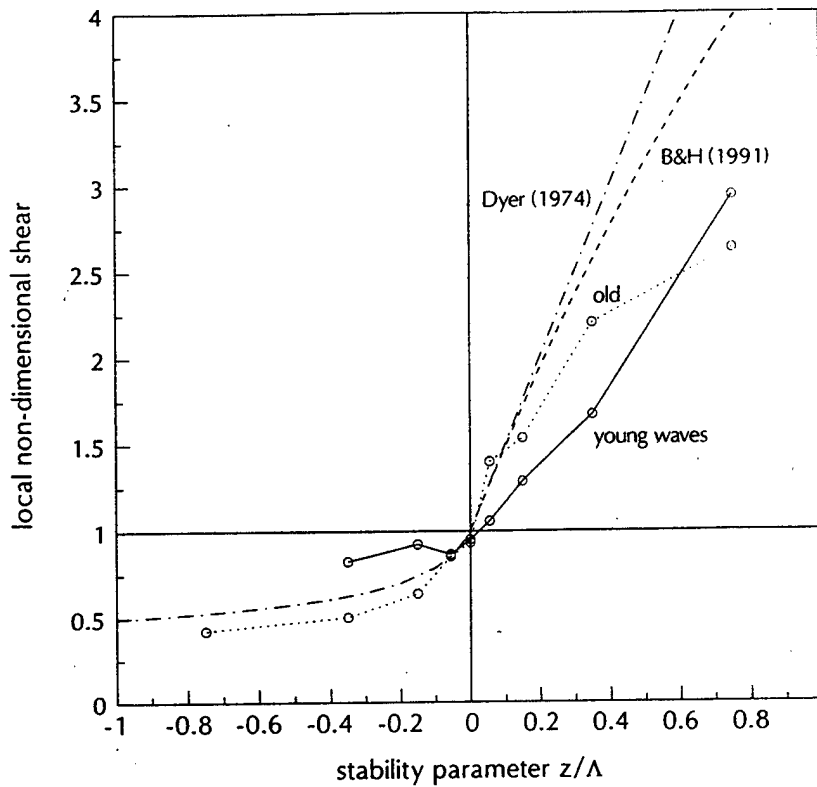
Figure 7. The mean local non-dimensional shear (ϕ_{ml}) for stability (z/Λ) categories (see text) for two wave-age (C_p/u_*) categories: (i) $C_p/u_* < 15$ (solid); and (ii) $C_p/u_* > 15$ (dotted), where C_p is the phase speed of the dominant wave mode. The dash-dot curve is the traditional Dyer (1974) parametrization. The dashed curve is the Beljaars and Holtslag (1991) formula.

than the Dyer (1974) formula (greater stress relative to the shear). It is not clear if the relatively weak shear observed here is related to the weak shear layer observed by Miller *et al.* (1997). For stable conditions, Eq. (8) predicts values of ϕ_{ml} significantly less than Dyer (1974) for values of z/Λ exceeding 0.2. The deviation of the non-dimensional shear from Dyer's formula is in the same direction as the Beljaars and Holtslag (1991) correction, but much greater in magnitude. Howell and Sun (1999) further document the overprediction of ϕ_m by traditional stability functions for strong stability, although the deviations from Dyer are greater in the present study.

To better isolate the potential influence of IBL depth and wave age on ϕ_{ml}, we calculated the residuals from the model, defined as the observed ϕ_{ml} minus Eqs. (7)–(8), and partitioned them by z/h and wave-age categories for unstable and stable periods. The observed ϕ_{ml} dataset includes all the on-shore and off-shore flow periods.

For unstable conditions, the ϕ_{ml} residuals increase with increasing z/h for $z/h < 1/3$ for all wave-age regimes except the youngest wave-age category (Table 1). The main effect here appears to be due to suppression of large convective eddies by shallow IBL depth (section 4(a)). For very shallow IBL depth ($z/h > 1/3$), ϕ_{ml} decreases with z/h. We attribute this to the elevated generation of turbulence. In unstable flow, there is no clear relationship between the ϕ_{ml} residuals and wave age.

The dependence of the unstable ϕ_{ml} residuals on z/h suggests including the dependence of the non-dimensional shear on z/h for convective IBLs. Here we choose the
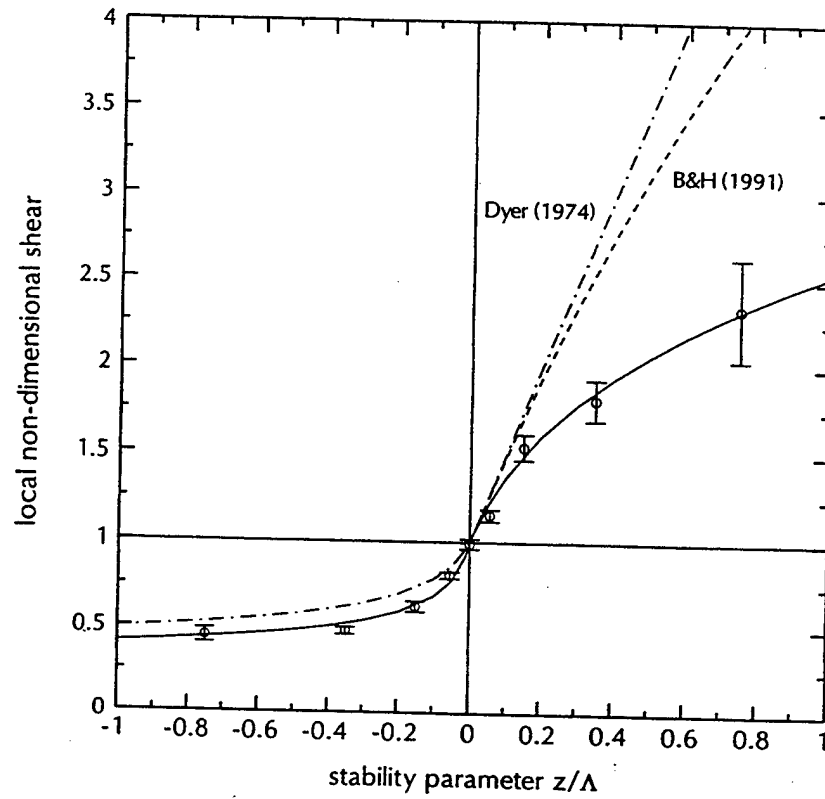
Figure 8. The mean and standard error of the local non-dimensional shear (ϕ_{ml}) for stability (z/Λ) categories (see text) for conditions where similarity theory is expected to be most applicable: (i) minimal advective effects (on-shore flow only); and (ii) relatively deep boundary layer depth ($z/h < 1/4$). The solid curve is a fit to the mean values given by Eqs. (7)–(8) with von Karman constant $\kappa = 0.39$. The dash-dot curve is the traditional Dyer (1974) parametrization. The dashed curve is the Beljaars and Holtslag (1991) formula.

TABLE 1. NON-DIMENSIONAL WIND SHEAR RESIDUALS (OBSERVED MINUS MODEL) FOR $z/\Lambda < 0$. THE COLUMNS ARE WAVE-AGE (C_P/u_*) CATEGORIES AND THE ROWS ARE z/h CATEGORIES. NUMBERS OF OBSERVATIONS ARE SHOWN IN PARENTHESIS

	5–10	10–15	15–20	20–25	25–30
0.32–1	−0.08 (20)	0.21 (13)	−0.06 (14)	−0.10 (09)	
0.1–0.32	0.01 (41)	0.30 (40)	0.00 (43)	−0.03 (17)	0.19 (04)
0.032–0.1	0.15 (08)	0.03 (39)	−0.02 (63)	0.01 (17)	−0.05 (06)
0.01–0.032	0.14 (07)	−0.03 (29)	−0.07 (34)	−0.09 (10)	

TABLE 2. AS TABLE 1 BUT FOR $z/\Lambda > 0$

	5–10	10–15	15–20	20–25	25–30
0.316–1	−0.56 (43)	−0.29 (43)	−0.17 (26)	0.23 (08)	0.80 (10)
0.1–0.316	−0.11 (39)	−0.06 (62)	−0.03 (30)	0.07 (18)	1.42 (06)
0.0316–0.1	−0.03 (28)	−0.02 (52)	0.13 (21)	0.22 (21)	0.47 (05)
0.01–0.0316	−0.08 (16)	0.17 (19)	0.37 (10)	0.25 (10)	0.44 (03)

74

form for the unstable case as

$$\phi_{ml} = \{1 - 35(z/\Lambda)\}^{-1/4} + (-z/\Lambda)^{1/2}(z/h)(1 - 1.5z/h). \tag{9}$$

The term $(z/h)(1 - 1.5z/h)$ augments ϕ_{ml} from the stability-dependence prediction for the parameter range $0 < z/h < 2/3$, and reduces ϕ_{ml} for $z/h > 2/3$. We include this expression mainly to clarify the observed z/h dependence of ϕ_{ml} in convective IBLs. A more precise calibration of this expression would require a larger dataset and more explicit determination of the boundary layer depth.

For stable conditions, the ϕ_{ml} residuals clearly increase with increasing wave age for the entire range of z/h (Table 2). Theoretically, the shear in the surface layer should adjust to the stress such that ϕ_{ml} is independent of wave age. Apparently with stable stratification, the adjustment time-scale of the weak turbulence may be too slow to maintain equilibrium with the changing surface state. Consequently, the assumptions required for similarity theory are not met. As a possible result, the flux-gradient relationship (ϕ_{ml}) at the observational level now depends on wave state. A simple model which demonstrates the observed dependence of the ϕ_{ml} residuals on wave age for the stable case is

$$\phi_{ml} = \{1 + 16(z/\Lambda)\}^{1/3} + (z/\Lambda)^2(C_p/u_* - 18)/20, \tag{10}$$

where the coefficients (18 and 20) were determined using the average residuals for the wave-age categories in Table 2. The wave-age term augments the stability-dependent prediction of ϕ_{ml} for older-wave fields ($C_p/u_* > 18$) and reduces ϕ_{ml} over younger waves. This model predicts zero wave-age influence for wave age equal to 18, which is smaller than the value of 25 thought to represent minimal wind–wave coupling (Volkov 1970).

In stable flow over young waves ($C_p/u_* < 20$), the ϕ_{ml} residuals clearly become more negative with increasing z/h (stronger stress relative to the shear), while over older waves the dependence on z/h is weak (Table 2). The decrease in ϕ_{ml} with increasing z/h in stable flow was noted in section 4(a), and attributed to a possible top-down nature of the turbulent transport. Table 2 shows that the combined influence of young waves and shallow stable IBL depths leads to the largest negative ϕ_{ml} residuals (smallest non-dimensional shear compared to Eqs. (7)–(8)) in this dataset. In this situation, the stress is large relative to the shear due to the influence of wind–wave coupling and the elevated generation of turbulence.

6. CONCLUSIONS

For convective internal boundary layers in the coastal zone, the non-dimensional wind shear is less than predicted by traditional similarity but increases with increasing z/h. The largest convective turbulent eddies are suppressed by the top of the internal boundary layer, leading to an increase in the non-dimensional shear with increasing z/h.

In stable internal boundary layers, elevated generation of turbulence can lead to an upside down boundary layer where the stress may even increase with height. As a result, the non-dimensional shear decreases with increasing z/h. This is apparently due to suppression of turbulence near the surface by the stratification and shear-generation of turbulence aloft. However, advection of stress may also be important.

In stable stratification, smaller non-dimensional shear is observed over young growing waves compared to older waves. We speculate that with the long adjustment time-scale and weaker turbulence associated with stable stratification, the mean shear in the

coastal zone does not completely adjust to the wind–wave coupling influence on the stress. In addition, the surface waves may effectively perturb the adjacent stable atmosphere, since vertical velocity fluctuations in a stratified atmosphere induce temperature-related pressure perturbations (such as internal gravity waves). Therefore, the non-dimensional shear depends on wave state, even though the observational levels are well above the wave boundary layer where individual eddies are coherent with surface waves. For convective and neutral conditions, wave state does not appear to have an influence on the non-dimensional shear.

A formulation for the non-dimensional shear (Eqs. (7)–(8)) in the marine surface layer is constructed as a function of the traditional stability parameter, based on data where the conditions required for application of similarity theory are expected to be met. Compared to the traditional land-based parametrization, the new formulation predicts slightly smaller non-dimensional shear for unstable conditions and significantly smaller non-dimensional shear for strong stability. The formulation is generalized to include the influence of internal boundary layer depth (Eq. (9)) and wave state (Eq. (10)). This formulation requires evaluation from a more extensive dataset to better isolate the influences of stability, internal boundary layer depth and wave state, that are sometimes inter-correlated. The formulation of the non-dimensional shear has been posed in terms of local scaling instead of Monin–Obukhov similarity theory. However, the distinction in the literature is not always clear, since the vertical flux divergence is usually not available and the difference between the flux at the observational level and the surface is not known.

APPENDIX

Elimination of records

The flux sampling errors and non-stationarity for momentum and buoyancy were evaluated following Vickers and Mahrt (1997b) and Mahrt (1998). All vertical levels of data for each one-hour time period with flux sampling errors exceeding prescribed thresholds for any of the 4 levels for either the momentum or the buoyancy flux were eliminated from further analysis. Using the notation in Vickers and Mahrt (1997b), the thresholds used were: (i) 6 for extreme subrecord flux outliers (event); (ii) 1 for the relative systematic flux error (RSE) associated with the flux on scales larger than the 10-minute average; (iii) 0.75 for the relative random flux error due to inadequate sample size (RFE); and (iv) 5 for non-stationarity of the flux (NR, defined in Mahrt 1998; his Eq. (11)). The averaging time-scale used in the flux sampling error analysis was: (i) 5-minutes for event and RFE, resulting in 12 independent estimates of the flux in each one-hour time period; (ii) 5- and 10-minute fluxes for estimation of the scale-dependence of the flux (RSE); and (iii) 100-second fluxes for the non-stationarity ratio NR. All the flux sampling criteria applied to the fluxes of momentum and buoyancy for all 4 vertical levels combined removed 35% of the one-hour time periods. Excluding data based on the flux sampling criteria reduced the scatter in the composited profiles of the wind stress and buoyancy flux. After the flux sampling screening, the final flux dataset consisted of

415 observations in off-shore flow and 483 observations in on-shore flow. No attempt was made to correct for potential flow distortion, which may contribute to scatter in the relationships.

REFERENCES

Barthelmie, R. J., Courtney, M. S., Højstrup, J. and Sanderhoff, P. 1994 'The Vindeby Project: A Description'. Report R-741(EN), Risø National Laboratory, DK4000, Roskilde, Denmark

Belcher, S. E. and Hunt, J. C. R. 1998 Turbulent flow over hills and waves. *Ann. Rev. Fluid Mech.*, **30**, 507–538

Beljaars, A. C. M. and Holtslag, A. A. M. 1991 Flux parametrization over land surfaces for atmospheric models. *J. Appl. Meteorol.*, **30**, 327–341

Bergström, H. and Smedman, A. 1995 Stably stratified flow in a marine atmospheric surface layer. *Boundary-Layer Meteorol.*, **72**, 239–265

Businger, J. A., Wyngaard, J. C., Izumi, Y. and Bradley, E. F. 1971 Flux profile relationships in the atmospheric surface layer. *J. Atmos. Sci.*, **28**, 181–189

Chalikov, D. V. and Belevich, M. Y. 1993 One-dimensional theory of the wave boundary layer. *Boundary-Layer Meteorol.*, **63**, 65–96

Chalikov, D. V. and Makin, V. K. 1991 Models of the wave boundary layer. *Boundary-Layer Meteorol.*, **56**, 83–99

Charnock, H. 1955 Wind stress over a water surface. *Q. J. R. Meteorol. Soc.*, **81**, 639–640

Davidson, K. L. 1974 Observational results on the influence of stability and wind–wave coupling on momentum transfer and turbulent fluctuations over ocean waves. *Boundary-Layer Meteorol.*, **6**, 305–331

Donelan, M. A. 1990 Air–sea interaction. Pp. 239–292 in *Ocean Engineering Science* Eds. B. LeMehaute and D. M. Hanes. John Wiley and Sons, New York, USA

Donelan, M. A., Dobson, F. W., Smith, S. D. and Anderson, R. J. 1993 On the dependence of sea surface roughness on wave development. *J. Phys. Oceanogr.*, **23**, 2143–2149

Dyer, A. J. 1974 A review of flux-profile relationships. *Boundary-Layer Meteorol.*, **7**, 363–372

Garratt, J. R. 1977 Review of drag coefficients over oceans and continents. *Mon. Weather Rev.*, **105**, 915–929

1990 The internal boundary layer—a review. *Boundary-Layer Meteorol.*, **50**, 171–203

Geernaert, G. L., Larsen, S. E. and Hansen, F. 1987 Measurements of the wind stress, heat flux and turbulence intensity during storm conditions over the North Sea. *J. Geophys. Res.*, **92**, 127–139

Grant, A. L. M. 1992 The structure of turbulence in the near-neutral atmospheric boundary layer. *J. Atmos. Sci.*, **49**, 226–239

Hare, J. E., Hara, T., Edson, J. B. and Wilczak, J. M. 1997 A similarity analysis of the structure of airflow over surface waves. *J. Phys. Oceanogr.*, **27**, 1018–1037

Högström, U. 1988 Non-dimensional wind and temperature profiles in the atmospheric surface layer: a re-evaluation. *Boundary-Layer Meteorol.*, **42**, 55–78

Højstrup, J. 1981 A simple model for the adjustment of velocity spectra in unstable conditions downstream of an abrupt change in roughness and heat flux. *Boundary-Layer Meteorol.*, **21**, 341–356

Højstrup, J., Edson, J., Hare, J., Courtney, M. S. and Sanderhoff, P. 1997 'The RASEX 1994 experiments'. Report R-788, Risø National Laboratory, Roskilde, Denmark

Howell, J. and Mahrt, L. 1997 Multiresolution flux decomposition. *Boundary-Layer Meteorol.*, **83**, 117–137

Howell, J. and Sun, J. 1999 Surface layer fluxes in stable conditions. *Boundary-Layer Meteorol.*, in press

Khanna, S. and Brasseur, J. G. 1997 Analysis of Monin–Obukhov similarity from large eddy simulation. *J. Fluid Mech.*, **345**, 251–286

Kitaigorodskii, S. A. 1970 *The physics of air–sea interaction.* Hydrometeorological Press, Lenningrad, Russia (English translation, 1973, available as TT 72-50062 from US National Technical Information Service, Springfield, VA 22151 USA)

Large, W. G., Morzel, J. and Crawford, G. B. 1995 Accounting for surface wave distortion of the marine wind profile in low-level ocean storms wind measurements. *J. Phys. Oceanogr.*, **25**, 2959–2971

Maat, N., Kraan, C. and Oost, W. A. 1991 The roughness of wind waves. *Boundary-Layer Meteorol.*, **54**, 89–103

Mahrt, L. 1998 Flux sampling errors for aircraft and towers. *J. Atmos. Oceanic Technol.*, **15**, 416–429

Mahrt, L., Vickers, D., Howell, J., Højstrup, J., Wilczak, J. A., Edson, J. and Hare, J. 1996 Sea surface drag coefficients in RASEX. *J. Geophys. Res.*, **101**, 14327–14335

Mahrt, L., Vickers, D., Edson, J., Sun, J., Højstrup, J., Hare, J. and Wilczak, J. A. 1998 Heat flux in the coastal zone. *Boundary-Layer Meteorol.*, **85**, 53–79

Makin, V. K., Kudryavtsev, V. N. and Mastenbroek, C. 1995 Drag of the sea surface. *Boundary-Layer Meteorol.*, **73**, 159–182

Miller, S., Friehe, C., Hristov, T., Edson, J. and Wetzel, S. 1997 'Wind and turbulence profiles in the surface layer over ocean waves'. Pp. 91–98 in Proceedings of the wind-over-wave couplings conference, University of Salford, April 1997. Eds. S. G. Sajjadi, N. H. Thomas and J. C. R. Hunt. Oxford University Press, New York, USA

Monin, A. S. and Obukhov, A. M. 1954 Basic laws of turbulent mixing in the atmosphere near the ground. *Tr. Akad. Nauk., SSSR Geophiz. Inst.*, No. 24 (151), 1963–1987

Nieuwstadt, F. T. M. 1984 The turbulent structure of the stable, nocturnal boundary layer. *J. Atmos. Sci.*, **41**, 2202–2216

Paulson, C. A. 1970 The mathematical representation of wind speed and temperature profiles in the unstable atmospheric surface layer. *J. Appl. Meteorol.*, **9**, 857–861

Peterson, E. W. 1969 Modification of mean flow and turbulent energy by a change in surface roughness under conditions of neutral stability. *Q. J. R. Meteorol. Soc.*, **95**, 561–575

Smedman, A. and Johansson, C. 1997 'Modifications of Monin–Obukhov similarity theory in unstable conditions'. Pp. 273–274 in Proceedings of the 12th Symposium on Boundary Layers and Turbulence, Vancouver. American Meteorological Society, Boston, USA

Smedman, A., Bergström, H. and Högström, U. 1995 Spectra, variance and length scales in a marine stable boundary layer dominated by a low level jet. *Boundary-Layer Meteorol.*, **76**, 211–232

Smith, S. D., Anderson, R. J., Oost, W. A., Kraan, C., Maat, N., DeCosmo, J., Katsaros, K. B., Davidson, K. L., Bumke, K., Hasse, L. and Chadwick, H. M. 1992 Sea surface wind stress and drag coefficients: the hexos results. *Boundary-Layer Meteorol.*, **60**, 109–142

Snyder, R. L., Dobson, F. W., Elliott, J. A. and Long, R. B. 1981 Array measurements of atmospheric pressure fluctuations above surface gravity waves. *J. Fluid Mech.*, **102**, 1–59

Sorbjan, Z. 1986 On similarity in the atmospheric boundary layer. *Boundary-Layer Meteorol.*, **34**, 377–397

Toba, Y. and Koga, M. 1986 A parameter describing overall conditions of wave breaking, white capping, sea-spray production and wind stress. Pp. 37–47 in *Oceanic whitecaps*. Eds. D. Reidel, E. C. Monahan and G. Mac Niocaill. D. Reidel Publishing Co., Dordrecht, the Netherlands

Vickers, D. and Mahrt, L. 1997a Fetch limited drag coefficients. *Boundary-Layer Meteorol.*, **85**, 53–79

1997b Quality control and flux sampling problems for tower and aircraft data. *J. Atmos. Oceanic Technol.*, **14**, 512–526

Volkov, Y. A. 1970 Turbulent flux of momentum and heat in the atmospheric surface layer over disturbed sea surface. *Izv. Atmos. Oceanic Phys.*, **6**, 770–774

Wetzel, S. W., Edson, J. B., Friehe, C., Hristov, T. and Miller, S. 1996 'An investigation of wave-induced momentum flux through phase averaging of open ocean wind and wave fields'. Summary Report, Marine Boundary Layer, Accelerated Research Initiative Experiment Review, October 28–30 1996. Scripps Institution of Oceanography, La Jolla, CA, USA

Wyngaard, J. C. 1973 'On surface-layer turbulence'. Pp. 101–148 in Workshop on micrometeorology, Boston. Ed. D. A. Haugen. American Meteorological Society, Boston, USA